Performance of Hydrostatic Machines

Extensive Measurement Report

INNAS

Breda, June 8, 2020

Contents

Nomenclature

Main symbols		
α	Volumetric expansion coefficient	[1/K]
η	Efficiency	[-]
θ	Temperature	[K]
ρ	Mass density	[kg/m^3]
ω	Rotational speed	[rad/s]
a_1	Correction factor	[-]
a_2	Correction factor	[-]
c	Heat capacity	[J/K]
$\bar{K}$	Secant bulk modulus	[Pa]
n	Rotational speed	[rpm]
p	Pressure	[Pa]
P	Power	[W]
Q	Flow rate	[m^3/s]
T	Measured torque	[Nm]
T_{th}	Theoretical torque	[Nm]
$\hat{T}$	Normalized torque	[-]
V	Volume	[m^3]
V_g	Geometric displacement volume	[m^3]
ΔV	V_g/z	[m^3]
z	Number of pistons or driving teeth	[-]

Subscripts	
1	Low pressure line
2	High pressure line
3	Drainage port
θ	Isothermal
h	Hydraulic
hm	Hydro-mechanical
$loss$	Losses
m	Mechanical
max	Maximum
min	Minimum
p	Isobaric
s	Isentropic
t	Total or overall
v	Isochoric

Superscripts	
M	Motor related
P	Pump related

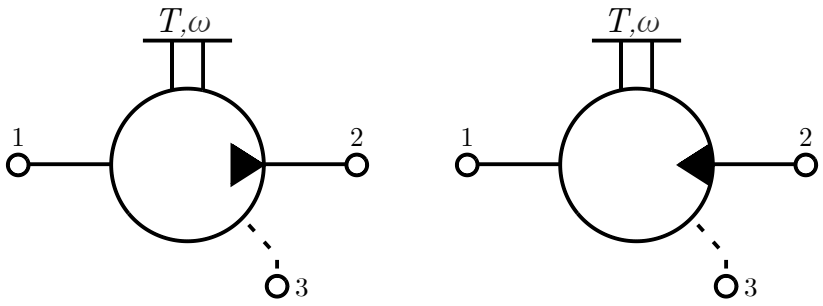

(a) *Pump* **(b)** *Motor*

Nomenclature of the subscripts regarding the oil properties for both pumps and motors (p, θ, Q, ρ). Subscript 1 refers to the low pressure line (input for pump, output for motor), subscript 2 refers to the high pressure line (output for pump, input for motor), and subscript 3 refers to the drainage port.

1 Introduction

This report contains results for performance measurements on eight different hydrostatic machines, of which some important specifications are shown in Table 1. In total there are three piston pumps, three piston motors, and two gear pumps. The piston machines have a number of pistons ranging from 7 to 24. From a physical point of view, the number of pistons is similar to the number of teeth in a gear pump, which is why they are also listed in the table. The geometric displacement volumes have been derived in accordance with Toet et al. [1], and range from 23.7 to 32.7 cc per revolution.

Each of the machines has been measured using the Innas test bench [2]. More on the test bench and the procedure of measuring the subjects is described in Section 2. In order to compute the results from these measurements, Section 3 explains the most important equations that were used. The actual results, and more on how to interpret them, are presented in Section 4.

Table 1: *Overview of the specifications of the tested machines, with the column P/M indicating whether it is a pump or motor by design, z the number of pistons or teeth, V_g the determined displacement volume, V_r the volume ratio $V_{min}/\Delta V$, and p_{max} and n_{max} the maximum pressure and speed operating condition specified by the manufacturer.*

Name	**P/M**	**Type**	z	V_g **[cc]**	V_r	p_{max} **[bar]**	n_{max} **[rpm]**
Rexroth A4FM28	Motor	Slipper, axial	9	27.75	0.78	400	4250
KYB MSF30	Motor	Slipper, axial	9	30.17	0.69	250	2000
Brevini SH11CM030	Motor	Bent-axis	7	31.89	0.44	430	4750
Rexroth A4FO28	Pump	Slipper, axial	9	27.87	0.78	400	3750
Moog RKP32	Pump	Slipper, radial	7	32.66	0.08	350	2750
Eckerle EIPH3-025	Pump	Internal gear	13	24.31	0.17	330	3200
Marzocchi ELI2-D-25.7	Pump	External gear	7	25.41	0.00	210	3000
Innas FC24	Pump	Floating cup	24	23.65	0.85	500	5000

2 Measurement Description

2.1 Measurement Setup

The Innas test bench can operate a hydrostatic machine at speeds ranging from 5000 rpm to less than 0.01 rpm, by using two different actuators. Figure 2 shows the most important mechanical components of the test bench. In the bottom left, we see where the pump or motor, that is being tested, will be coupled to the main axle. Moving to the right on the axle, we first see a torque and a speed sensor, followed by two different sized sprockets. An electric linear actuator can wrap around one of these sprockets to drive the pump or motor consistently at speeds from around 1 rpm to less than 0.01 rpm. After the sprockets, we first see a coupling to switch between operation by the linear actuator or by the large electric motor that follows directly after it. This electric motor can rotate the test subject at any speed between 10 and 5000 rpm. On the other end of the electric motor, a second hydrostatic machine can be attached to recirculate the power that the test subject generates. This machine is operated as a pump in case the specimen to be tested is a motor, and vice versa.

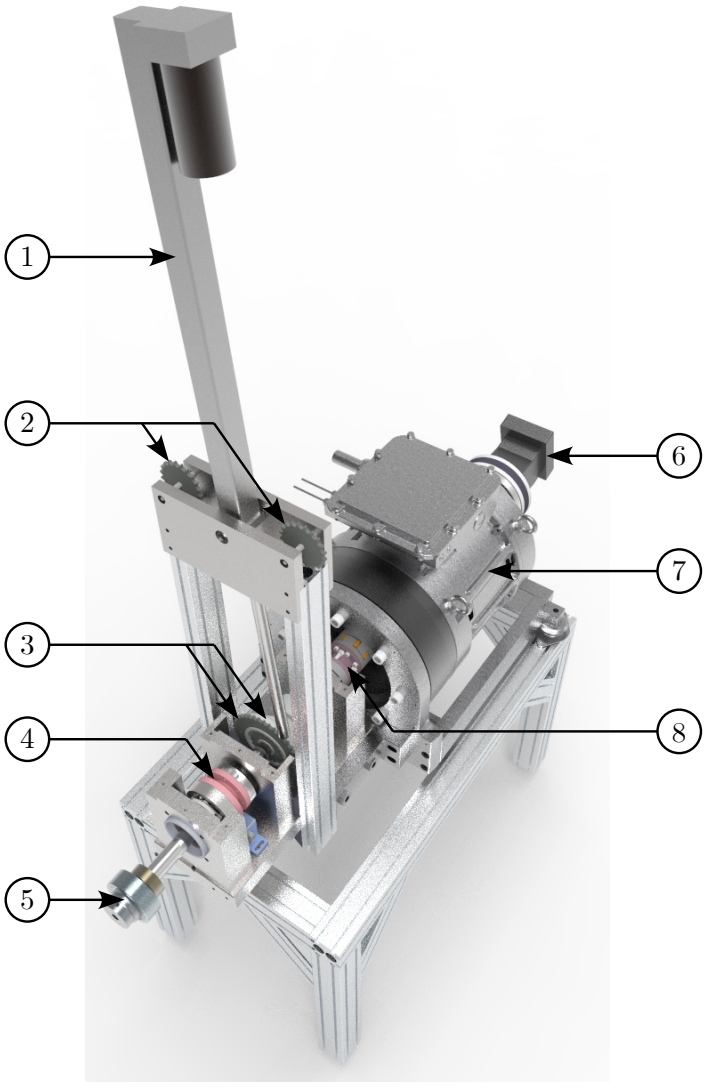

1. Linear actuator with build-in position sensor
2. Sprockets for the counter weight, one for each direction of rotation
3. Sprockets for very low speed tests, one with 60 teeth, one with 36 teeth
4. Torque and speed sensor
5. Coupling for the pump or motor to be tested
6. Hydraulic motor or pump for power recirculation
7. Frequency controlled, water cooled electric motor
8. Switchable coupling

Figure 2: *Render of the test bench used to drive the test subjects.*

During operation, the different sensors in the mechanical part and in the hydraulic circuit will measure the following parameters:

- Torque on the main axle, T
- Speed of the main axle, ω
- Pressure on the low pressure side, high pressure side, and in the housing, p_1, p_2, p_3
- Oil temperature at the low pressure side, high pressure side, and leakage, $\theta_1, \theta_2, \theta_3$
- Main flow rate at the high pressure side, Q_2
- Leakage flow rate, Q_3

More information about the test bench can be found in Appendix A. This appendix shows a simplified version of the hydraulic circuit including the most important hydraulic parts, and a list of sensors that have been used for the measurements.

2.2 Procedure

Before each measurement, the test subject is driven at a reasonable speed and pressure level, to allow it and the oil to warm up. When the oil and the machine are at a steady temperature (around 50°C in the measurements in this report), the parameters listed above are measured during operation of the pump or motor at a number of predetermined speeds and pressure levels. This normal test procedure is in accordance with ISO4409:2019 [3] and will additionally be used to determine the geometrical displacement in accordance with Toet et al. [1].

After the high speed performance tests, the low speed tests can be performed. By shifting a coupling, the low speed actuator can be connected and activated. This integration ensures that the test object can remain on the test bench, including all the sensors and hydraulic lines. Additionally, the oil and the pump or motor that is being tested remain at warm operating conditions. During the low speed measurements, the linear actuator first makes a downward stroke followed by an upward stroke. Since the test subject is not removed from the bench between these two strokes, it is tested both as a motor and as a pump.

The low speed measurements allow a precise comparison of individual test runs. Figure 3 shows two separate tests of the same pump at the same operating conditions. The resemblance of the two measurements shows that the results are very repeatable. Furthermore, the figure shows a significant variation of the torque losses at different angels. This is partly due to the limited number of pistons ($z = 9$ for the example in Figure 3), and partly due to small differences in the tribological interfaces.

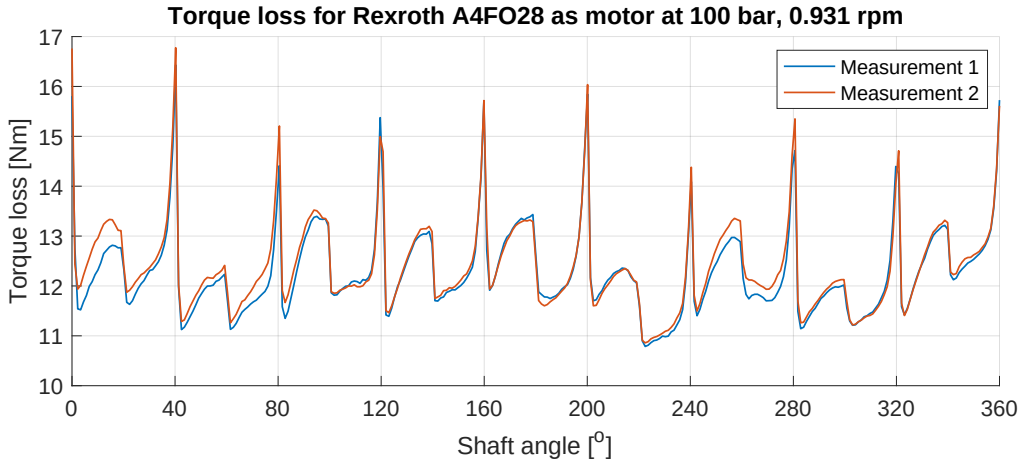

Figure 3: *Torque loss for two different low speed tests of the same machine at equal test conditions.*

3 Theory and Equations

During the analysis of the different machines, we will look at several results from the measurements. The three most important quantities, that will be used to describe the performance of the test subject, are the overall efficiency η_t, torque loss T_{loss}, and leakage Q_3. This section describes how the efficiency and torque loss can be derived from the measured data, while the leakage is measured directly.

It is important to note that several definitions in this section are derived by Achten et al. [4], and differ from the current standard for measuring and presenting the performance of hydrostatic machines as described in ISO4409:2019 [3] and ISO4391 [5]. The difference can be found in the compressibility correction factors a_1 and a_2.

3.1 Overall Efficiency

To determine the efficiency of a hydrostatic machine, we first need to calculate the mechanical power P_m and hydraulic power P_h:

$$P_m = T\omega \tag{1}$$
$$P_h = p_2 Q_2 a_2 - p_1 Q_1 \tag{2}$$

In these equations, T and ω are the measured shaft speed and torque, p_i and Q_i are the pressure and flow rate of oil through line i (1 = low pressure line, 2 = high pressure line), and a_2 is a correction factor to account for the compressibility of oil at high operating pressures. As derived by Achten et al. [4]:

$$a_2 = 1 + \frac{p_2}{2\bar{K}_s} \tag{3}$$

with $\bar{K}_s$ the isentropic bulk modulus of the used oil. In the case of a pump, mechanical power is converted into hydraulic power, while a motor works the other way around. The overall efficiency of the machine is the ratio at which power is converted:

$$\eta_t^P = \frac{P_h}{P_m} = \frac{p_2 Q_2 a_2 - p_1 Q_1}{T\omega} \tag{4}$$
$$\eta_t^M = \frac{P_m}{P_h} = \frac{T\omega}{p_2 Q_2 a_2 - p_1 Q_1} \tag{5}$$

3.2 Torque Loss

The amount of torque that is lost during operation can be calculated by comparing the measured torque T to the theoretical torque T_{th}:

$$T_{loss}^P = T - T_{th} \tag{6}$$
$$T_{loss}^M = T_{th} - T \tag{7}$$

The difference in sign is similar to the difference in sign for the efficiencies: torque drives a pump to generate a pressure and flow, while a pressure and flow drives a motor to generate torque. The theoretical torque will thus be lower than the measured torque for pumps, to overcome friction and pressure ripples, and the other way around for motors. The theoretical torque can be calculated using:

$$T_{th} = \frac{(p_2 - p_1)V_g}{2\pi} a_1 \tag{8}$$

with V_g the derived geometric displacement volume, and a_1 a correction factor to account for the compressibility of oil at high operating pressures. As derived by Achten et al. [4]:

$$a_1 = 1 - \left(\frac{1}{2} + \frac{V_{min}}{\Delta V}\right)\frac{\Delta p}{\bar{K}_s} \tag{9}$$

with V_{min} the dead volume per cylinder, and ΔV the geometric displacement volume per piston (V_g/z). In order to compare the torque loss of pumps and motors of different sizes, the torque loss can be normalized. The normalized torque loss is defined as $\hat{T}_{loss}$ as follows:

$$\hat{T}^P_{loss} = 1 - \frac{T_{th}}{T} \tag{10}$$

$$\hat{T}^M_{loss} = 1 - \frac{T}{T_{th}} \tag{11}$$

3.3 Oil Model

For calculation of the correction factors a_1 and a_2, the isentropic bulk modulus $\bar{K}_s$ is needed. This modulus has been measured by Karjalainen et al. [6] for the oil *Shell Tellus46* at 40°C and 70°C. Since the measurements in this report are conducted with this oil at a temperature of roughly 50°C and pressure levels ranging to 400 bar, the average between the two measurements by Karjalainen et al. [6] at 200 bar will be used as a constant:

$$\bar{K}_s = 1.76 \cdot 10^9 \text{ [Pa]} \tag{12}$$

Another important parameter in (2) is the flow rate on the low pressure side of the test subject, Q_1. Due to the possibility of cavitation, this flow rate can not be measured directly, and needs to be derived using the measured rates Q_2 and Q_3, and the isothermal bulk modulus $\bar{K}_\theta$ and volumetric thermal expansion coefficient α:

$$Q^P_1 = Q_2\left[1 - \frac{p_1 - p_2}{\bar{K}_\theta} + \alpha(\theta_1 - \theta_2)\right] + Q_3\left[1 - \frac{p_1 - p_3}{\bar{K}_\theta} + \alpha(\theta_1 - \theta_3)\right] \tag{13}$$

$$Q^M_1 = Q_2\left[1 - \frac{p_1 - p_2}{\bar{K}_\theta} + \alpha(\theta_1 - \theta_2)\right] - Q_3\left[1 - \frac{p_1 - p_3}{\bar{K}_\theta} + \alpha(\theta_1 - \theta_3)\right] \tag{14}$$

From the Maxwell equations, we know that the ratio between isentropic and isothermal bulk modulus is equal to the ratio between the isobaric and isochoric heat capacities (c_p and c_v respectively). From Hodges [7] we know that this ratio is roughly 1.15 and the volumetric thermal expansion coefficient is roughly 0.00075 per K:

$$\frac{\bar{K}_s}{\bar{K}_\theta} = \frac{c_p}{c_v} \approx 1.15 \text{ [-]}, \qquad \alpha \approx 0.00075 \text{ [1/K]} \tag{15}$$

Alternatively, a more detailed oil model could be used to determine the bulk modulus more accurately. Appendix B shows that this has little impact on the measurement results, and concludes that using a single constant bulk modulus will suffice in the deriving the performance of the machines tested in this report.

4 Measurement Results

This section shows and compares the results from the performance measurements for the different machines. Please note that, due to a difference in the limits for each of the machines, some of the machines will have less data points at certain operating conditions than other machines. Furthermore, Appendix C.1 shows a full measurement report for each of the individual test subjects in terms of torque loss, leakage, power loss, and efficiency. Appendix C.2 shows the comparison of the different machines at other pressure levels than shown in this section.

4.1 Overall Efficiency

The overall efficiency of the machines was determined using (4) and (5). The results for different shaft speeds and an operating pressure of 200 bar are shown in Figure 4. For all of the machines, the efficiency shows the same trend for an increasing shaft speed. At low operating speeds, the efficiency is low as well. As the machine starts rotating faster, the efficiency increases rapidly, until a maximum is reached somewhere between 1000 and 2000 rpm. As the shaft speed increases further, the efficiency decreases at a much lower rate.

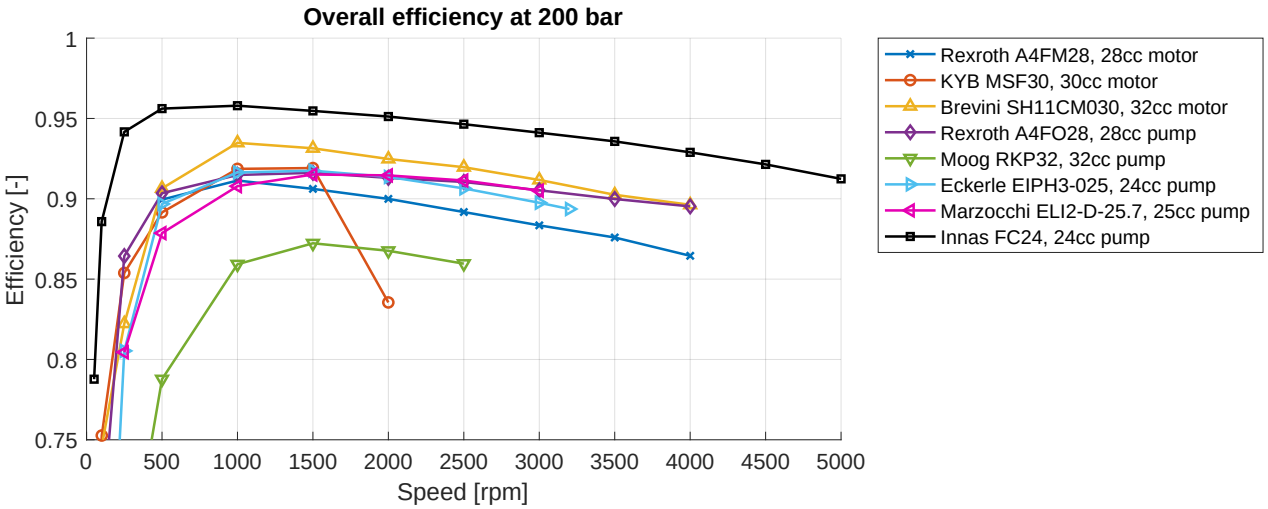

Figure 4: *Comparison between the measured power loss for all of the machines with $p_2 = 200$ bar.*

At this particular pressure level, the highest peak efficiency of almost 0.96 was realized by the Innas pump at 1000 rpm, while the Moog pump had the lowest peak efficiency of 0.87 at 1500 rpm. One exceptional point in Figure 4 is the 2000 rpm measurement of the KYB motor. The efficiency of this machine decreases much faster than is to be expected from following the results from lower measurements. In this case, the machine in question is running near its maximum rated operating speed, which as we will later see causes a lot of additional torque loss and leakage as well.

4.2 Torque Loss

Using (6) and (7), the difference between the theoretical torque and the measured torque has been calculated for each of the measured machines. To properly compare machines of different sizes, these losses have been normalized as described by (10) and (11). Figure 5 shows the normalized torque losses at 200 bar on both a linear and a logarithmic scale. The linear scaled plot mainly shows the losses at normal operating conditions, while the logarithmic plot provides some insight into the losses during low speed operation (e.g. startup condition).

Overall the torque loss shows a similar trend for each of the machines, regardless whether they are operated as a motor or a pump. At speeds below 1 rpm (see logarithmic plot), the torque loss appears to be constant. At some point, the torque loss starts to quickly decrease for increasing shaft speeds, until a minimum is reached. From this speed onwards, the torque loss increases again, but at a slower rate. This trend is very much in accordance with the Stribeck curve, and the three sections describe the transition from coulomb friction (boundary lubrication), to mixed friction, and viscous friction (hydrodynamic lubrication), respectively.

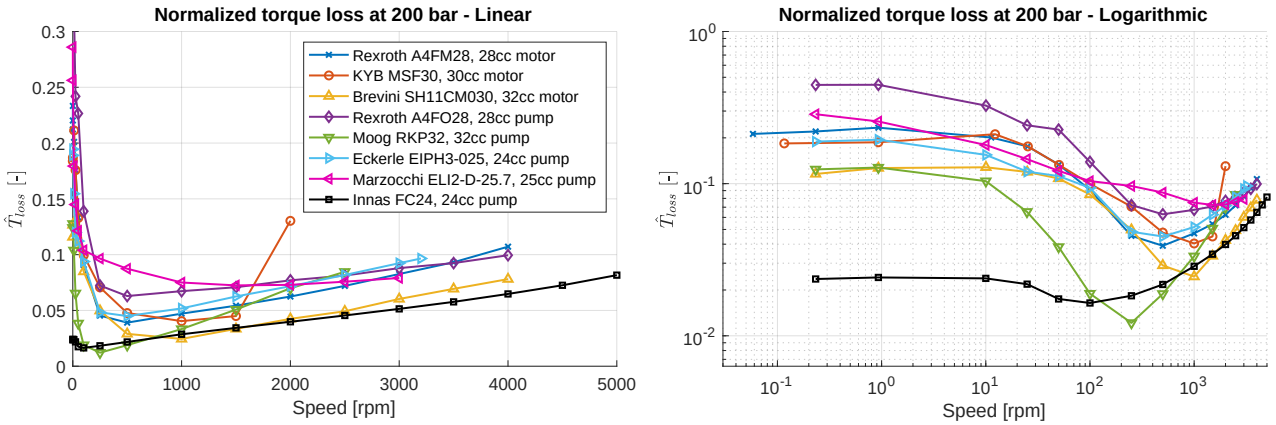

Figure 5: *Comparison between the normalized torque losses for all of the machines with $p_2 = 200$ bar.*

In the linear plot of Figure 5, we see that at this pressure level the three motors have very similar torque losses for the normal operating speeds. Furthermore, the logarithmic plot shows that the Brevini motor outperforms the other two motors in the low speed range, where it has less torque loss than the KYB and the Rexroth motor.

The five pumps show larger differences with respect to each other. Overall, the Innas pump has the lowest torque loss at this pressure, especially in the low speed range. This can be explained by the fact that this is a floating cup type pump, which has almost no contact between the piston and the cylinder, and thus very little coulomb friction. In the viscous friction section, the torque loss in the Rexroth, the Eckerle, and the Innas pump increase at roughly the same rate. The torque loss for the Moog pump increases at a faster rate, while the torque loss of the Marzocchi seems relatively constant at higher operating speeds.

During the low speed measurements, the test bench allows for testing each machine during pump operation as well as motor operation, regardless of the direction it should on paper be driven in. However, since the Eckerle pump is an internal gear pump, its design does not allow it to be tested as a motor so these tests has not been conducted. Figure 6 shows the normalized torques for the machines in motor operation (left side of the figure), and in pump operation (right side of the figure). Figure 5 has shown that the torque loss is more or less constant at operating speeds below 1 rpm, due to coulomb friction. The width of the shapes at the end of each of the pressure levels in Figure 6 shows the range between the minimum and maximum measured torque loss at any of these low speeds.

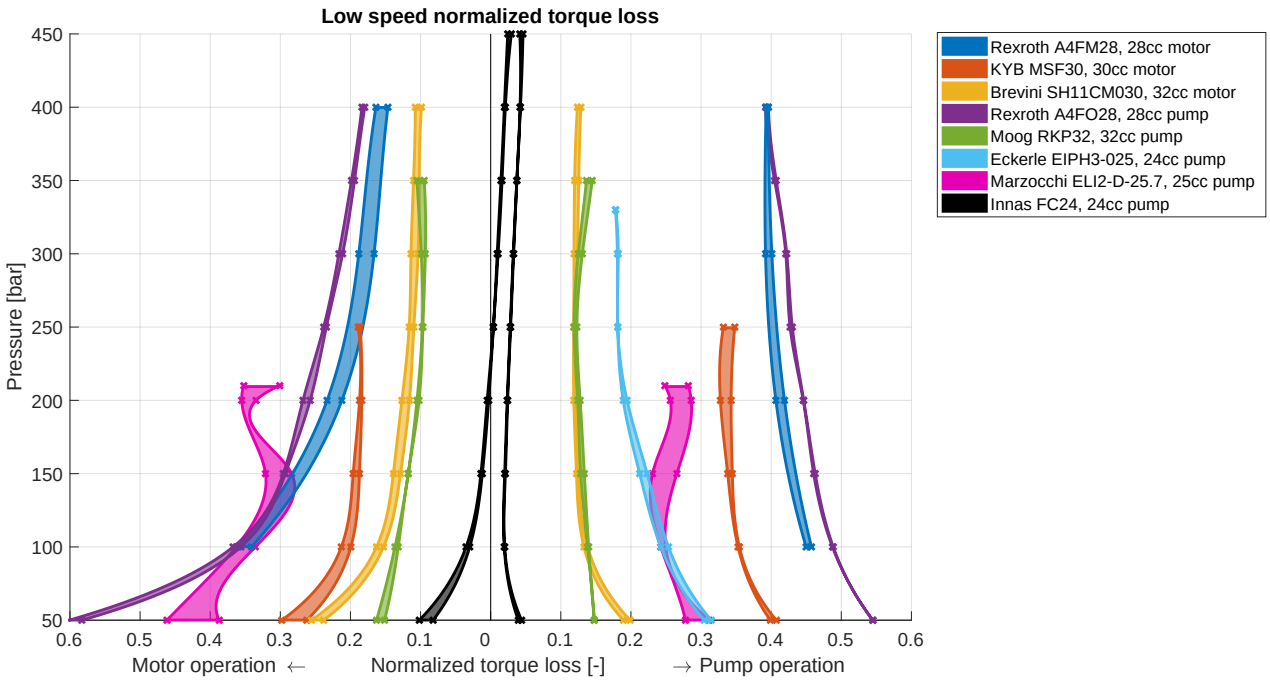

Figure 6: *Normalized torque loss with respect to pressure p_2 during the measurements at less than 1 rpm for the different machines, driven both as a motor (left side) and as a pump (right side). The width at each pressure indicates the range in the torque losses between the different measurements for this machine.*

In Figure 6, we see that for most piston machines the torque loss due to coulomb friction is larger when it is driven as a pump. The exception being the Brevini machine, which has more or less the same torque loss for both directions. This can be explained by the direction in which the piston moves during the high pressure stroke. When operated as a pump, the piston pushes the barrel to the portplate during the high pressure stroke, increasing the friction between those two surfaces and therefore the torque loss. When operated as a motor, the piston pulls the barrel away from the portplate, decreasing the friction.

The highest amount of torque loss can be found on the Rexroth pump, which loses up to 60% of torque at these operating speeds. It is worth noting that the two Rexroth units are, apart from the silencing grooves in the portplates, the same machine. This can be confirmed by comparing the torque loss for the two machines when they are driven in the same direction.

The normalized torque loss of the Innas pump during low speed motor operation becomes less than zero. In other words, more torque was delivered to the shaft than the theoretical maximum. At these low speeds, the leakage will be larger than the amount of oil that is displaced. In this case, an additional pump is used to provide the right pressure level. Unfortunately, equations (13) and (14) no longer apply in this situation, making it impossible to derive the overall efficiency. This approach is chosen to emulate the behaviour of the machines as part of a larger hydraulic network, which is often the case. It is currently hypothesized that the pressure delivered by this supply pump has an effect on the torque on the test specimens shaft as well. Further research will be needed to determine why this is the case, and what this means for further analyses.

The results shown in Figure 6 show average values of the normalized torque loss. However, at these low speeds there is a big difference in torque loss between different angular positions of the units shaft. Figure 7 and Figure 8 shows the measured torque divided the theoretical torque, with respect to the angular position of the shaft. In the case of pumps, this normalized torque is larger than 1,

meaning that a certain amount of additional torque needed to overcome the friction. Figure 7 shows that some of the tested specimens needed as much as 80% extra torque to be operated at this speed. In the case of motors, the normalized torque is less than 1, meaning that less torque is provided by the supplied oil. Figure 8 shows a torque loss as much as 30% for one of the units.

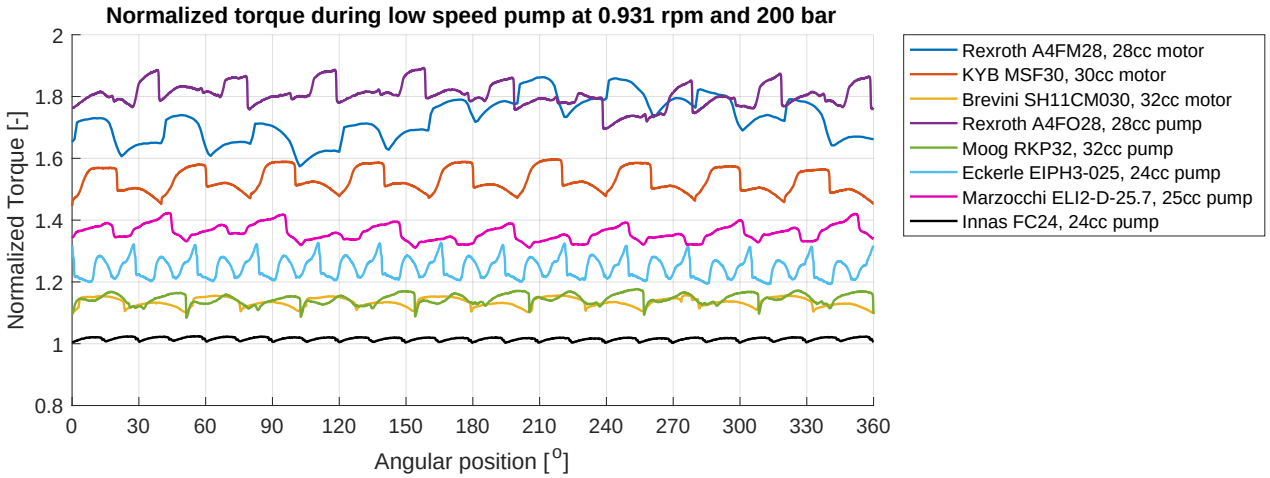

Figure 7: *Normalized torque for different units operated as pump, at pressure $p_2 = 200$ bar and speed 0.931 rpm.*

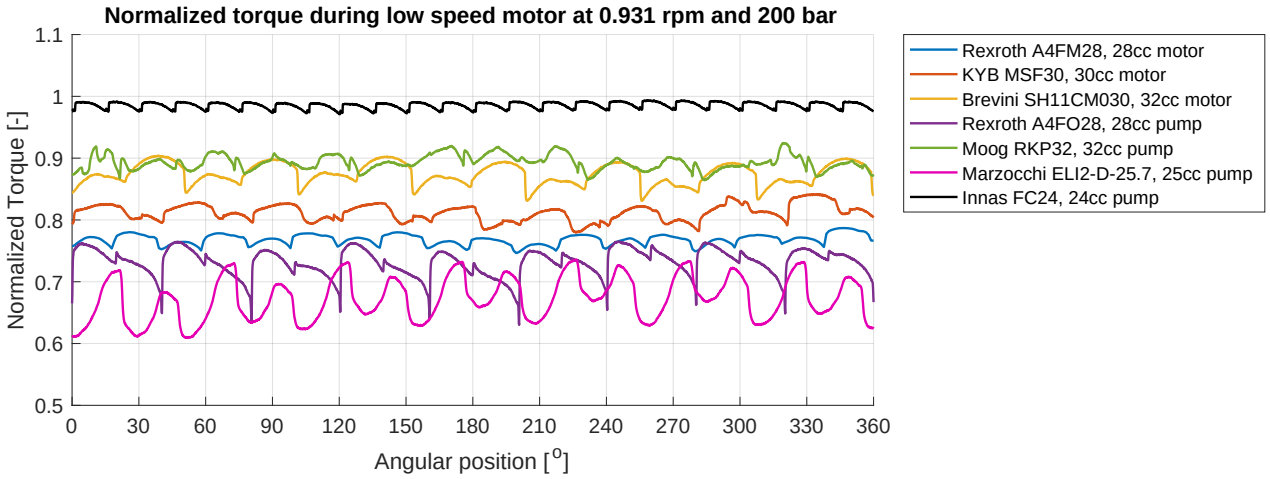

Figure 8: *Normalized torque for different units operated as motor, at pressure $p_2 = 200$ bar and speed 0.931 rpm.*

4.3 Leakage Flow Rate

The leakage flow rate from the rotary group to the pump or motor housing is measured directly in the test bench. Please note that the gear pumps do not have an external leakage port, so the leakage can not be measured. Internal leakage will affect the total output flow rate, so it will be visible in the efficiency calculations. Figure 9 shows the measured leakage for each of the other machines at 200 bar. In this figure, we see that for most machines, the leakage increases slightly for increasing shaft speeds. This makes sense, since increasing the shaft speed will increase the amount of displaced oil linearly. However, the relatively constant leakage flow rates at low operating speeds suggest that it does not only depend on shaft speed. A constant leak flow generally means that the gap through which oil leaks does not change very much, indicating that this is probably caused by the precision with which the parts have been made and how accurately they fit together.

Similar to the low speed torque losses, Figure 10 shows the average leakage flow rate for the measurements at speeds less than 1 rpm. The width of some of the shapes in Figure 10 shows that there is quite some difference in leakage between the different measurements. Main factors for these larger ranges seem to be the oil temperature (which is difficult to control during these very low speed measurement), and the case pressure (mainly the case for the Moog pump).

Even though there is a significant spread in the flow rate measurements at different low speeds, Figure 10 shows that the leakage is generally higher during motor operation for most machines. When operated as a pump, the piston pushes the barrel to the portplate during the high pressure stroke, decreasing the size of this leakage path. When operated as a motor, the piston pulls the barrel away from the portplate, which allows for more leakage. The exceptions being the Innas pump, which has more or less equal leakage for both directions, and the Brevini motor, which has more leakage when driven as a pump than when driven as a motor. Interestingly, where the two Rexroth units showed similar torque losses, there is a large difference between their leakage flow rate, which can most likely be appointed to the difference in portplates. Furthermore, one can see a clear wave pattern in the results of the Innas pump. Since these measurements take a very long time, and only little oil flows through the machine, the temperature of the house of the machine decreases over time. This has a large effect on the viscosity of the leakage oil, causing oil to flow slower at lower temperatures. When the measurements are conducted in succession, the house and the oil need to be heated between them.

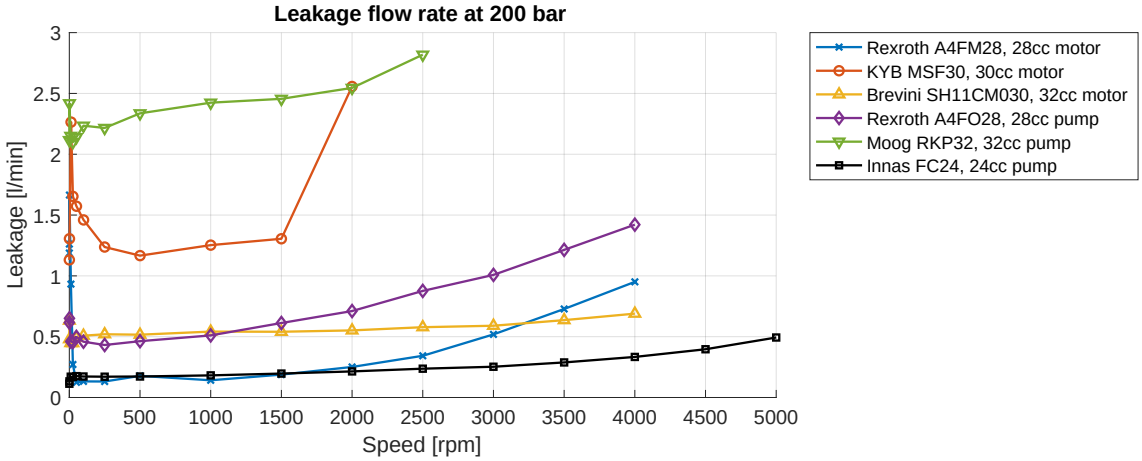

Figure 9: *Comparison between the measured leakage flow rate for all of the machines with $p_2 = 200$ bar.*

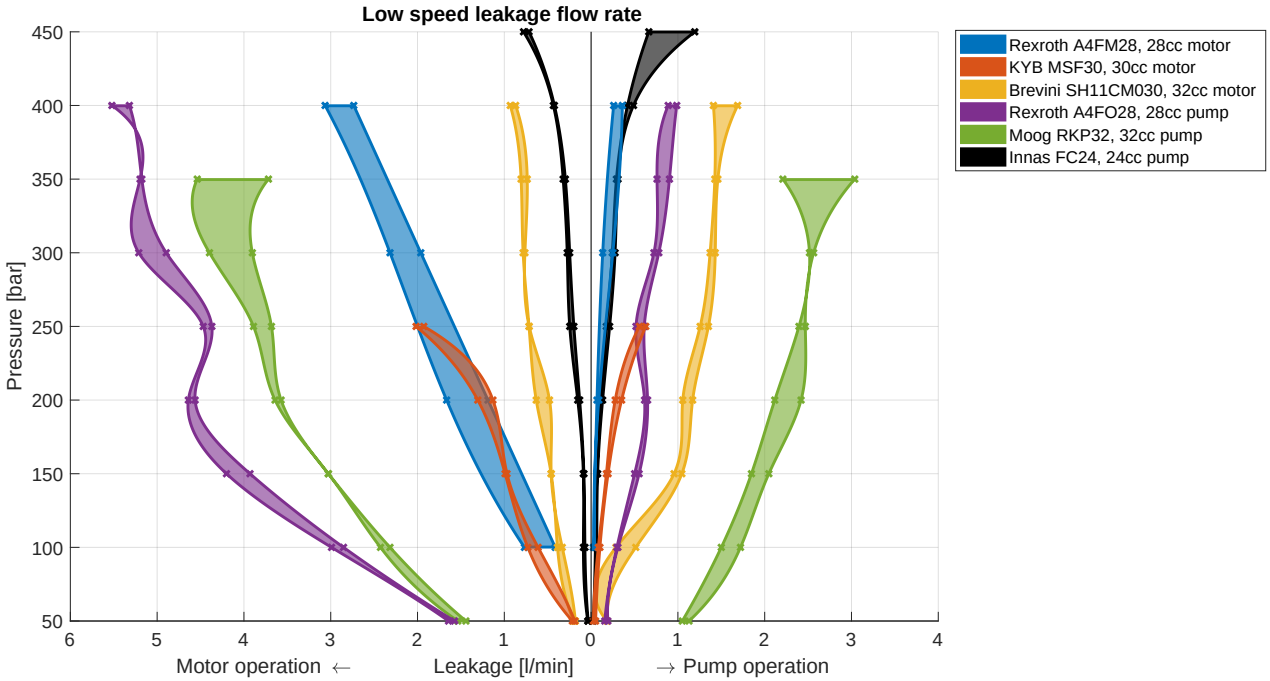

Figure 10: *Average leakage flow rate during the measurements at less than 1 rpm for the different machines, driven both as a motor (left side) and as a pump (right side). The width at each pressure indicates the range in the leakage between the different measurements for this machine.*

5 Conclusion

The performance of eight different hydrostatic machines has been measured on the Innas test bench. The results of these measurements have been used to calculate the overall efficiencies, torque loss, and leakage flow rate of each of the machines at pressure levels ranging from 50 to 450 bar. Due to the unique test bench, the machines could be measured at shaft speeds ranging from 0.058 to 4400 rpm.

From comparing the overall efficiency of the different machines, it has been found that each of the test subject follows roughly the same trend. At low operating speeds, the efficiency is low as well. The efficiency increases rapidly for increasing shaft speeds, until a maximum is reached. As the shaft speed increases further, the efficiency decreases at a much lower rate. The exact location of the maximum efficiency point differs per machine per pressure level. Due to the use of an additional pump to account for high leakages during some of the low speed operation measurements, the efficiencies could not be calculated in these situations.

The torque loss has been analysed using both the high speed and low speed measurements. The results showed a typical Stribeck curve: constant torque loss at very low speeds (coulomb friction), followed by a fast decrease in friction for increasing speeds (mixed friction), and a slower increase after passing a certain shaft speed (viscous friction).

The leakage flow rate of all the machines has been measured as well. During measurements in which the leakage was found to be larger than the displaced oil, an additional pump was used to emulate the machine as part of a larger hydraulic circuit. From the results, it was found that the leakage increases for higher shaft speeds, but remains somewhat constant at lower shaft speeds. This has been appointed to the accuracy with which the components of the machines fit together: less precise fits generally means more leakage. During the low speed measurements, we have seen that there are other factors that influence the leakage of some machines more than others, in particular the oil temperature and case pressure.

The low speed measurements have shown a significant difference in torque loss and leakage between the direction in which the machines were driven. When operated as a pump, the piston pushes the barrel to the portplate during the high pressure stroke, decreasing the distance between those two surfaces. This results in higher friction, but less leakage flow rate. When operated as a motor, the piston pulls the barrel away from the portplate during the high pressure stroke, increasing the distance between those two surfaces. This results in lower friction, but more leakage.

References

[1] G. Toet, J. Johnson, et al. "The Determination of the Theoretical Stroke Volume of Hydrostatic Positive Displacement Pumps and Motors from Volumetric Measurements". In: *Energies* 12.3 (2019), p. 415.

[2] P. Achten, J. Potma, and S. Eggenkamp. "A New Hydraulic Pump and Motor Test Bench for Extremely Low Operating Speeds". In: *ASME/BATH 2017 Symposium on Fluid Power and Motion Control*. American Society of Mechanical Engineers. 2017, V001T01A015–V001T01A015.

[3] ISO4409:2019. *Hydraulic Fluid Power, Positive Displacement Pumps, Motors and Integral Trans- missions; Methods of Testing and Presenting Basic Steady State Performance*. Internatio- nal Organization for Standardization. 2019.

[4] P. Achten, R. Mommers, et al. "Measuring the Losses of Hydrostatic Pumps and Motors; A Critcal Review of ISO4409:2007". In: *BATH/ASME 2019 Symposium on Fluid Power and Motion Control*. American Society of Mechanical Engineers. 2019.

[5] ISO4391. *Hydraulic fluid power - Pumps, motors and integral transmissions - Parameter definitions and letter symbols*. Internatio- nal Organization for Standardization. 1983.

[6] J.-P. Karjalainen, R. Karjalainen, and K. Huhtala. "Measuring and modelling hydraulic fluid dynamics at high pressure Accurate and simple approach". In: *International Journal of Fluid Power* 13.2 (2012), pp. 51–59.

[7] P. Hodges. *Hydraulic fluids*. Butterworth-Heinemann, 1996.

[8] H. H. Ku et al. "Notes on the use of propagation of error formulas". In: *Journal of Research of the National Bureau of Standards* 70.4 (1966).

[9] K. Witt. "Die Berechnung physikalischer und thermodynamischer Kennwerte von Druckflüssig- keiten, sowie die Bestimmung des Gesamtwirkungsgrades an Pumpen unter Berücksichtigung der Thermodynamik für die Druckflüssigkeit". In: (1974).

[10] H. Gholizadeh, R. Burton, and G. Schoenau. "Fluid bulk modulus: a literature survey". In: *International Journal of Fluid Power* 12.3 (2011), pp. 5–15.

A Test Bench Specifications

A.1 Hydraulic Circuit

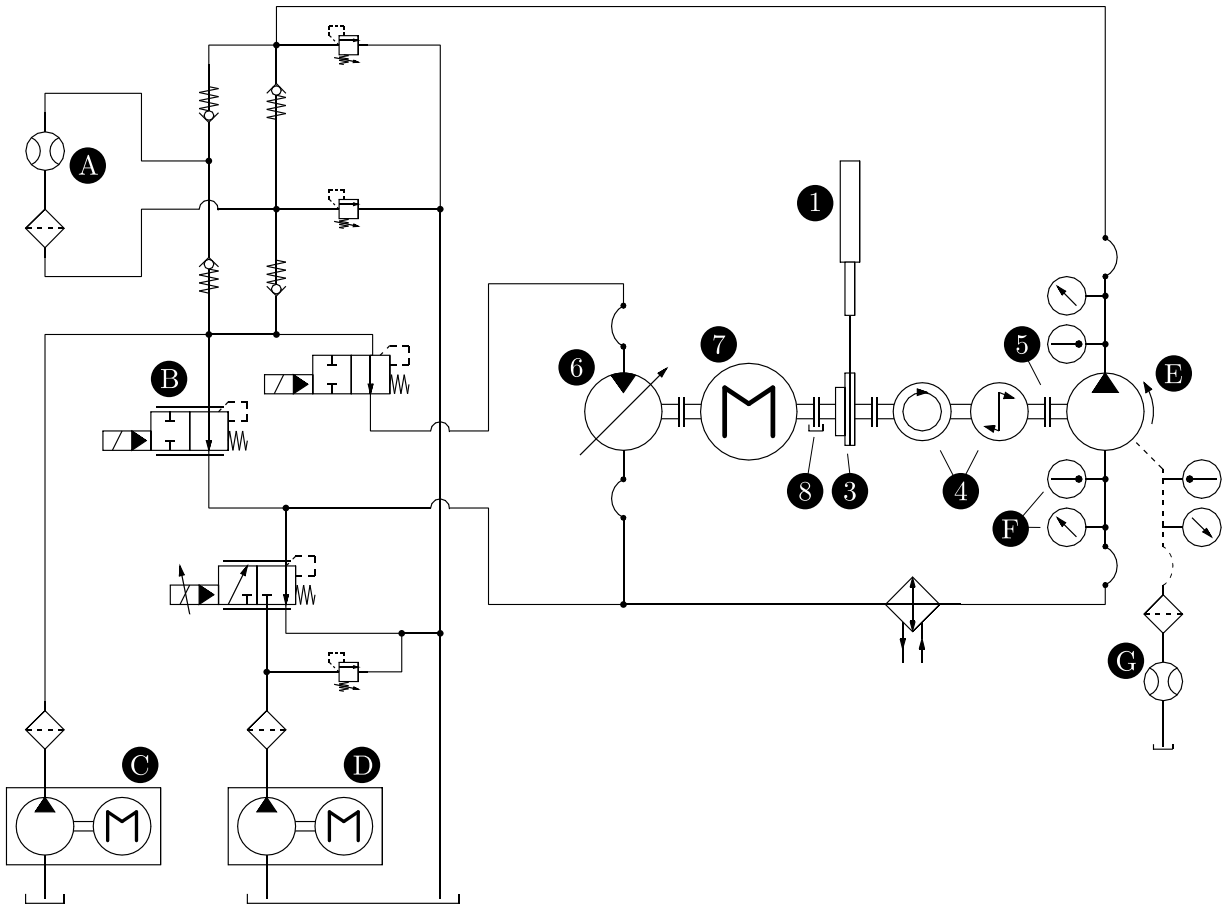

1. Linear actuator incl. position sensor
3. Sprockets for very low speed tests
4. Torque and speed sensor
5. Coupling for the test subject
6. Hydraulic motor or pump for power recirculation
7. Frequency controlled, water cooled electric motor
8. Switchable coupling

A. Flow meter high pressure flow
B. Load valve
C. Supply pump high pressure side
D. Supply pump low pressure side
E. Pump or motor to be tested
F. Temperature and pressure sensors (on each of the lines)
G. Flow meter case drain flow

Figure A.1: *Simplified sketch of the hydraulic circuit that was used during the tests. The numbers in the circuit correspond with the numbers in the render of the test bench shown in Figure 2.*

A.2 Sensor Information

Table A.1: *List of sensors in the test bench and their specifications. Relative accuracy is given with respect to either the full scale operation (FSO), or measured value (MV).*

Variable	Symbol	Sensor	Range		Accuracy	
Torque	T	Kistler 4541A / 4550A500	-500...500	Nm	0.05%	FSO
Low pressures	p_1,p_3	Honeywell TJE 500 psig	0...34.5	bar	0.1%	FSO
High pressure	p_2	Honeywell STJE 7500 psig	0...517.1	bar	0.05%	FSO
Flow rate	Q_2	VSE RS 400/32	1.0...400	l/min	0.5%	MV
Leakage flow	Q_3	VSE VSI 0.1/16	0.01...10	l/min	0.3%	MV
Temperature	t_1,t_2,t_3	Testo type 13 PT100 class B	-50...+400	°C	0.3 °C	

A.3 Measurement Error

The accuracy data of the different sensors is used to perform an analysis of the error propagation in the calculated total efficiency, power loss and torque loss, using variance formula [8]. The figures below show the resulting error bars for these variables, for the measurements of the floating cup unit at pressures $p_2 = 100, 200, 300, 400$ bar. These figures are followed by the maximum error for each of the measured pressure levels.

The error bars for the calculated overall efficiency of the Innas FC24 is shown in Figure A.2. The maximum error for all measured pressure levels is shown in Figure A.3. The maximum error figure shows that for a pressure of 250 bar or more, the error in the calculated efficiency increases to roughly 0.005. Between 100 bar and 250 bar, the maximum error is slightly larger, but never more than 0.0065. The measurements at 50 bar can have a measurement error of up to 0.01 at the low operating speeds. This maximum error decreases to about 0.007 at maximum speed.

The error bars for the calculated total power loss of the Innas FC24 is shown in Figure A.4. The maximum error for all measured pressure levels is shown in Figure A.5. This figure shows that the error increases close to linear with speed. The largest maximum error for the shown operating points in Figure A.4 is less than 380 W, at 5000 rpm, 400 bar. Note that this is a relative error of roughly 6% of the calculated power loss. If we look at the relative error of all the points, we find that for pressure levels of 200 bar and higher, the maximum error becomes about 6% of the calculated power loss at 5000 rpm. At lower pressure levels, the maximum error at 5000 rpm is less. Furthermore, this relative error is largest at lower speed (somewhere between 100 and 1000 rpm for most pressures). The maximum error on the calculated power loss for the 50 bar measurements shows an especially large amount of uncertainty at low speeds. Since so little power lost, the error can become almost three times as large as the measured power loss.

The calculation of the torque loss depends heavily on the theoretic torque, which is calculated using the displacement volume V_g (estimated in accordance with Toet et al. [1]) and the ratio between dead volume and displacement volume V_r (estimated using available drawings of the machine). Since both these parameters are thought not to be very accurate, they are included in the torque losses. Figure A.6 shows the error bars for the calculated torque loss of the Innas FC24, when assuming $V_g \pm 0.05$ cc/rev and $V_r \pm 0.05$. Figure A.7 shows that these errors do not depend on the speed.

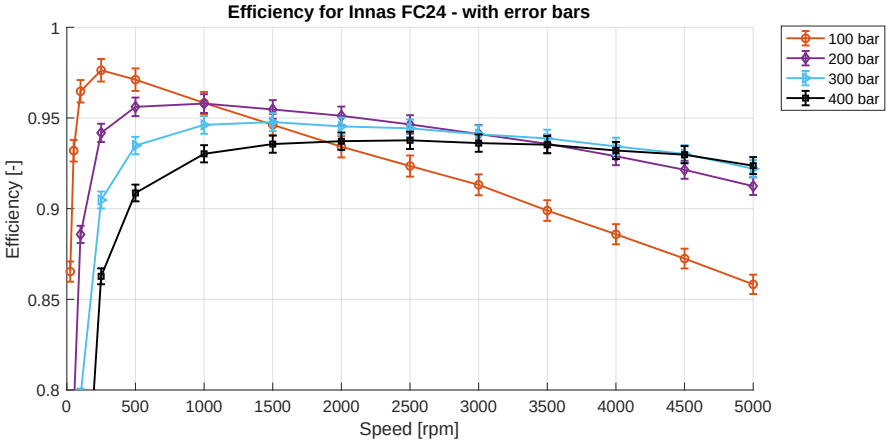

Figure A.2: *Efficiencies of the Innas FC24 measurements at 100, 200, 300, and 400 bar, with error bars that indicate the maximum measurement error.*

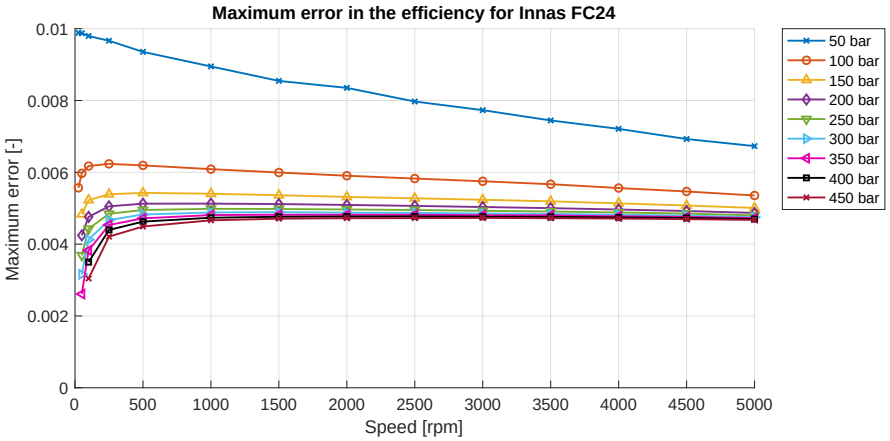

Figure A.3: *Maximum measurement error for the calculated efficiency of the Innas FC24.*

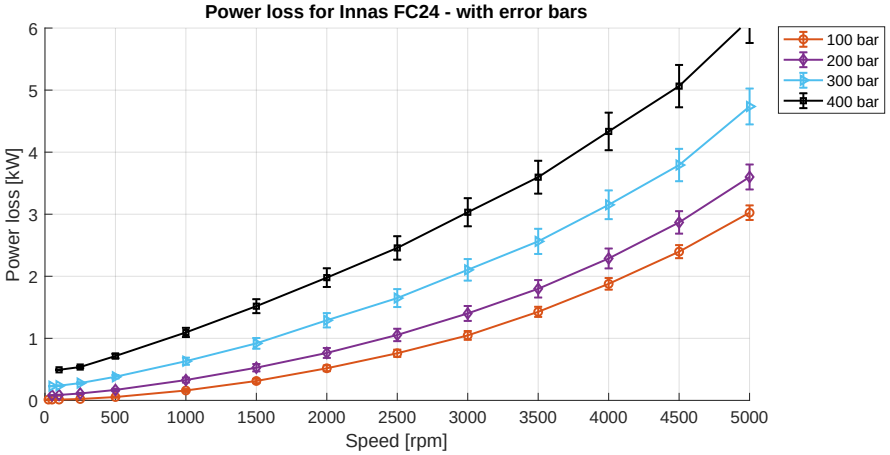

Figure A.4: *Power loss of the Innas FC24 measurements at 100, 200, 300, and 400 bar, with error bars that indicate the maximum measurement error.*

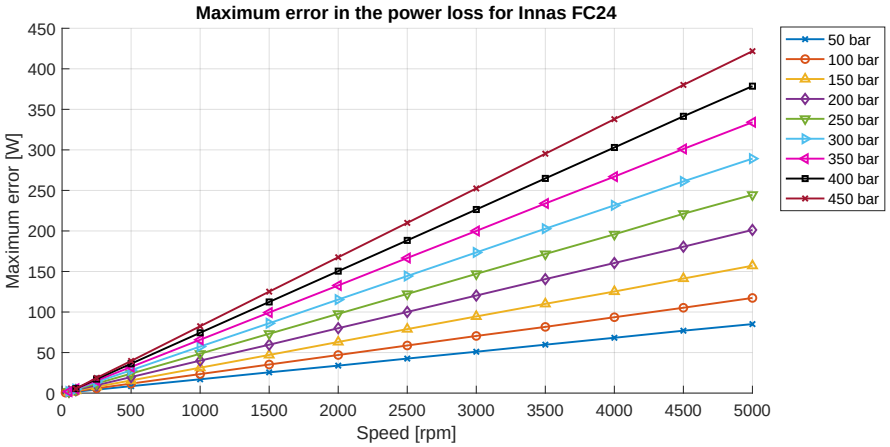

Figure A.5: *Maximum measurement error for the calculated power loss of the Innas FC24.*

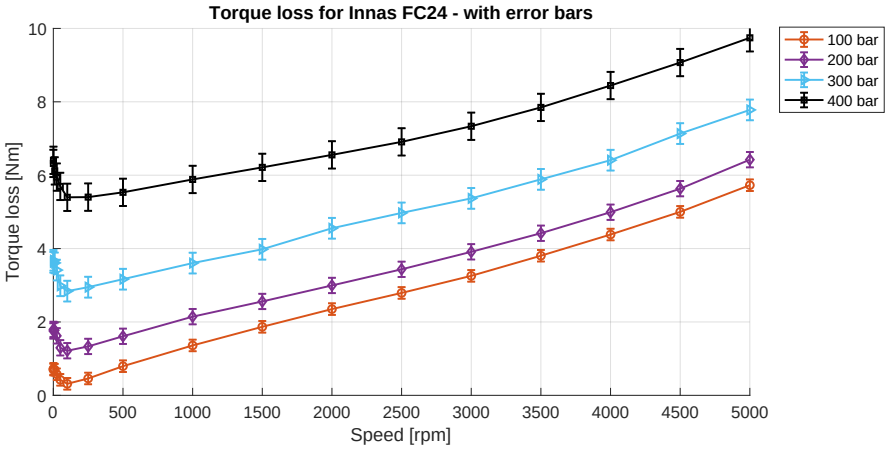

Figure A.6: *Torque loss of the Innas FC24 measurements at 100, 200, 300, and 400 bar, with error bars that indicate the maximum measurement error. In this figure,* $\epsilon_{V_g} = 0.05$ *cc/rev and* $\epsilon_{V_r} = 0.05$.

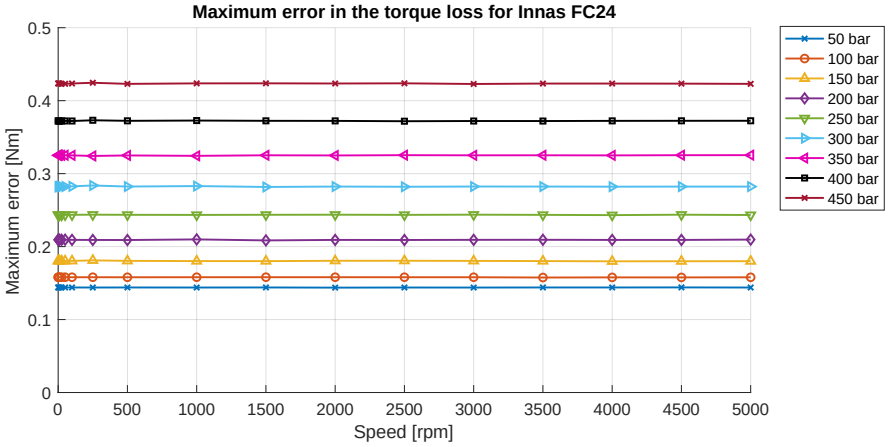

Figure A.7: *Maximum measurement error for the calculated torque loss of the Innas FC24.*

B Sensitivity Analyses of the Bulk Modulus

The results shown in this report are all based on the equations introduced in Section 3. This section explains that the overall efficiency and torque loss should be corrected for the compressibility. To this end, two correction factors a_1 and a_2 are introduced, which both depend on the isentropic bulk modulus $\bar{K}_s$. Additionally, the same bulk modulus is used to determine the low pressure flow Q_1. For simplicity, a constant value of $1.76 \cdot 10^9$ Pa has been used for this modulus.

To determine how sensitive the results are to this arbitrary choice of a constant bulk modulus, we will need a detailed oil model. Witt [9] describes a detailed model for *DTE25* which is very similar to the *Tellus46* that was used. From the model, we can obtain a mass density for the oil at any pressure and temperature. These densities can then be used to derive a more accurate low pressure flow and isentropic bulk modulus. From (4) and (5), we can derive:

$$\hat{\eta}_t^P = \frac{p_2 Q_2 \hat{a}_2 - p_1 \hat{Q}_1}{T\omega} \tag{B.1}$$

$$\hat{\eta}_t^M = \frac{T\omega}{p_2 Q_2 \hat{a}_2 - p_1 \hat{Q}_1} \tag{B.2}$$

In these equations, $\hat{Q}_1$, $\hat{a}_2$, and $\hat{\eta}_t$ are the low pressure flow rate, correction factor, and overall efficiency, calculated using the oil density model from Witt [9] instead of using a constant bulk modulus.

B.1 Low Pressure Flow Rate

Deriving a more accurate low pressure flow rate $\hat{Q}_1$ is very straightforward. Since we now have a model for the mass density, (13) and (14) can be simplified to:

$$\rho(p_1, \theta_1)\hat{Q}_1^P = \rho(p_2, \theta_2)Q_2 + \rho(p_3, \theta_3)Q_3 \tag{B.3}$$

$$\rho(p_1, \theta_1)\hat{Q}_1^M = \rho(p_2, \theta_2)Q_2 - \rho(p_3, \theta_3)Q_3 \tag{B.4}$$

in which ρ is a function of pressure and temperature (the model).

B.2 Correction Factors

Determining a more accurate correction factor a_2 is less straightforward. The process involves deriving isentropic properties from the measured results. For the bulk modulus, we know [10]:

$$K_i = \rho \left(\frac{\partial p}{\partial \rho} \right)_i \tag{B.5}$$

in which i is the thermodynamic variable that is kept constant: $i = \theta$ for isothermal, and $i = s$ for isentropic processes. By using the partial derivative of pressure with respect to density, we get the so-called tangent bulk modulus. In each of the equations in Section 3 however, the secant bulk modulus is used (as shown by the bar above the $\bar{K}$):

$$\bar{K}_i = \rho \left(\frac{\Delta p}{\Delta \rho} \right)_i \tag{B.6}$$

which can be seen as a linearisation between the changes in pressure and mass density. Figure B.1 shows some isothermal lines for the mass density as a function of pressure. The two red lines illustrate the process of determining the tangent bulk modulus at 400 bar and the secant bulk modulus for a

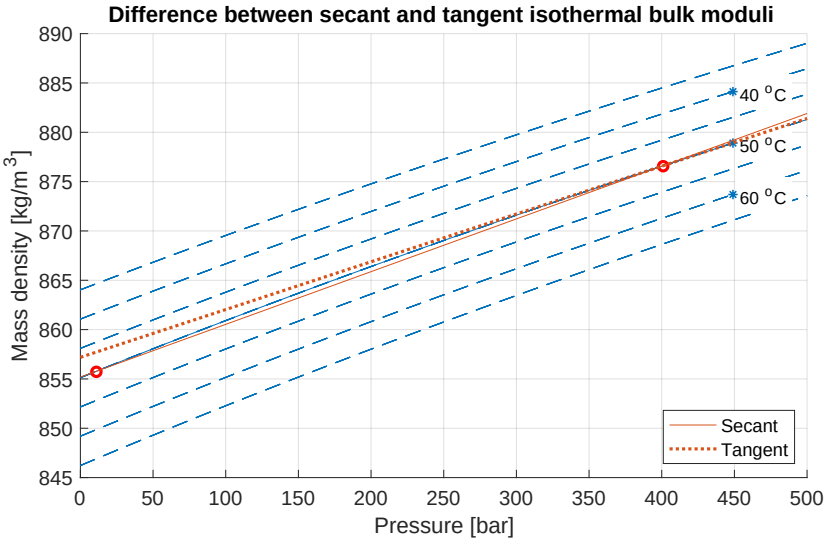

Figure B.1: *Difference between determining the secant and tangent isothermal bulk modulus for the used oil model at 50°C.*

pressure increase from 10 to 400 bar. Please note that although a_2 in (3) uses the secant bulk modulus for one pressure (p_2), it actually describes the difference between this pressure and atmospheric pressure ($\Delta p = p_2 - p_{atm} = p_2$).

The equations in Section 3 use the isentropic secant bulk modulus. Since the measurement have definitely not been an isentropic process, we need to correct for the increase in oil temperature due to losses. This can be done by looking at the measured pressure and temperature in a Mollier diagram. Figure B.2 shows this diagram and contains the specific enthalpy and entropy of the three mass flows for the Innas FC24 pump at 400 bar and 2500 rpm. The lines from bottom to top are isobars, while the lines from left to right are isotherms. Please note that it is impossible to calculate absolute enthalpy or entropy. The values in a Mollier diagram always give the change of these parameters with respect to another state, in this case the enthalpy and entropy at p_{atm} at 0 °C.

In order to find the mass density of the oil in case of an isentropic process, we can draw a vertical line (constant entropy) from the point of the low pressure flow Q_1 until it reaches the pressure p_2. From the isotherms, we can now read the temperature the oil would have if the process would have been isentropic. The difference between the actual temperature and the isentropic temperature will be caused by energy losses. Note that since entropy never decreases, in case of a motor, the Q_1 point will be to the right of the Q_2 point, and we need to determine the temperature of Q_1 for an isentropic pressure decrease from p_2 to p_1.

Now that the temperatures for isentropic processes are known, the secant isentropic bulk modulus can be calculated as follows:

$$\bar{K}_s^P = \hat{\rho}_2 \frac{p_2 - p_1}{\hat{\rho}_2 - \rho_1} \tag{B.7}$$

$$\bar{K}_s^M = \rho_2 \frac{p_2 - p_1}{\rho_2 - \hat{\rho}_1} \tag{B.8}$$

with $\hat{\rho}_i$ the mass density at pressure i and derived isentropic temperature. Implementing these more accurate values for the bulk modulus in (3) will results in a new estimation of a_2, which we will further refer to as $\hat{a}_2$.

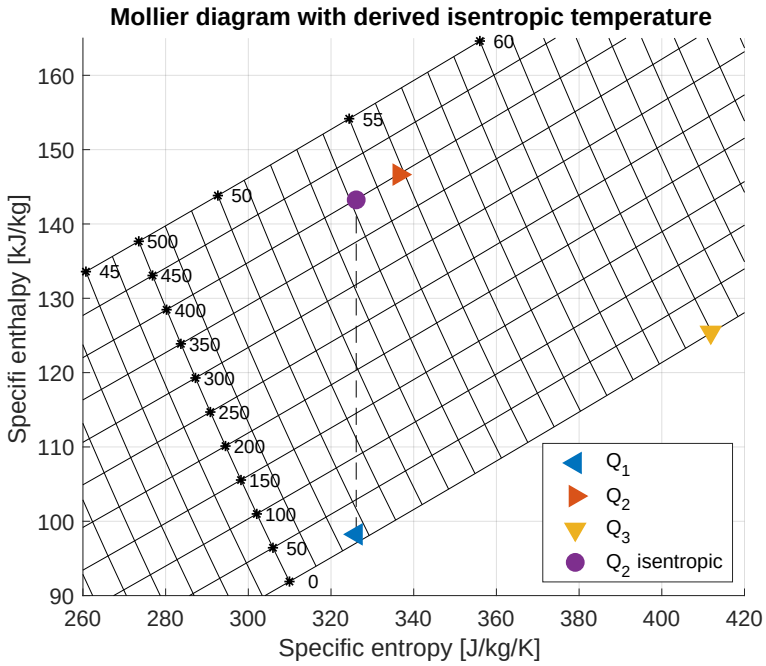

Figure B.2: *Mollier diagram containing the specific enthalpy and entropy of the three measured flows for the FC24 at 400 bar, 2500 rpm. The lines from bottom to top are isobars, while the lines from left to right are isotherms. Please note that the specific enthalpy and entropy are shown with respect to p_{atm} at 0 °C. The dashed line indicates the isentropic pressure and temperature increase from p_1 to p_2, ending in the isentropic oil properties for Q_2.*

B.3 Comparison and Conclusion

Firstly, a comparison between the overall efficiencies that were calculated using a constant bulk modulus and a variable bulk modulus ($\eta_t - \hat{\eta}_t$) is presented for two of the test subjects in Figure B.3. Overall, this figure shows that the difference between both calculations is very small, for these two machines it is never more than 0.0007. Furthermore, we see that the line at which both calculations agree, the zero contour, lies around 200 bar in both figures. Since we assumed the constant bulk modulus in Section 3.3 to be the average bulk modulus at 200 bar from Karjalainen et al. [6], the model seems to agree with this assumption.

Secondly, the difference in torque loss is investigated by understanding the influence of a change in the bulk modulus. Equations (8) and (9) show that the bulk modulus affects the theoretical torque via correction factor a_1 only. Using the same notation as before, the correction factor resulting from calculations using the oil density model will be referred to as $\hat{a}_1$. Figure B.4 shows the effect of the volume ratio $V_{min}/\Delta V$ and the pressure difference $\Delta p = p_2 - p_1$ on the ratio $\hat{a}_1/a_1$. From the almost identical figures, it can be concluded that the difference between the two methods is very small. In the extreme case of ratio $V_{min}/\Delta V = 8$ and $\Delta p = 500$, this ratio was found to still be relatively small: $\hat{a_1}/a_1 = 1.0182$.

In conclusion, it is found that the alleged increase in accuracy gained by using a detailed oil density model to determine the bulk modulus is probably negligible compared to the accuracy of the measurement results. For the sake of clarity as well as simplicity, the use of a constant value for the isentropic bulk modulus during the calculation of hydrostatic performances will suffice.

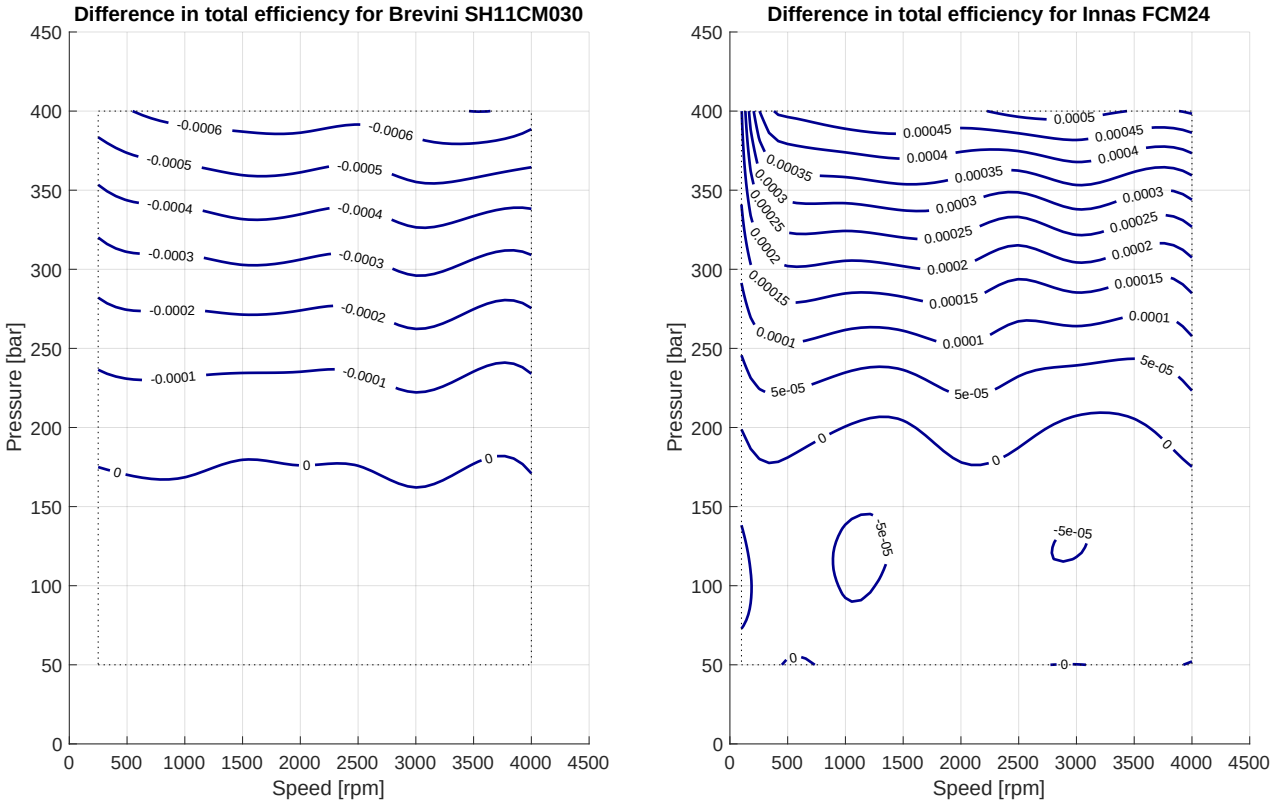

Figure B.3: *Difference in efficiency calculations between using a constant bulk modulus and using a variable bulk modulus from a mass density model (values are $\eta_t - \hat{\eta}_t$).*

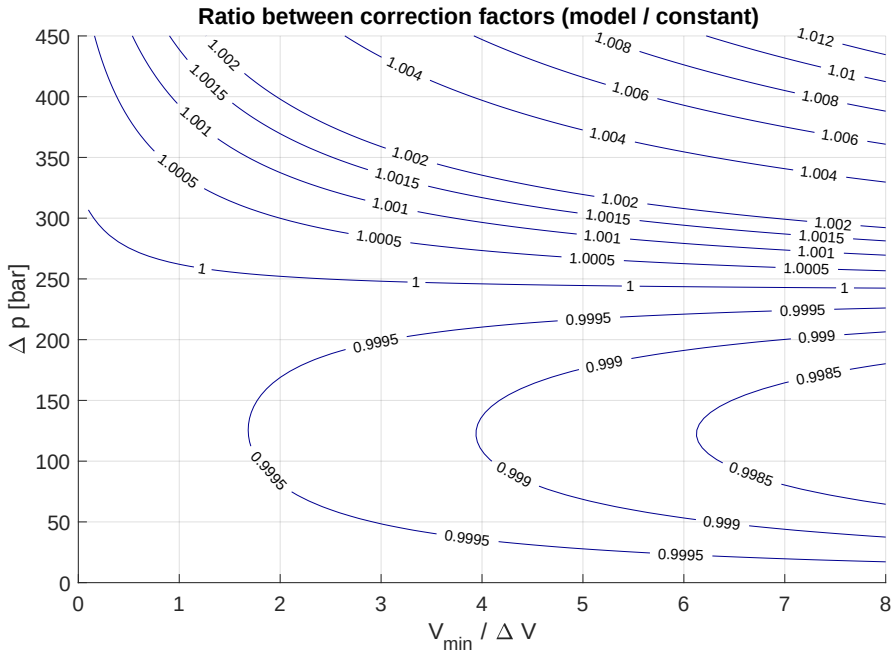

Figure B.4: *Ratio between correction factors for the theoretical torque between using a variable bulk modulus from a mass density model and using a constant bulk modulus (values are $\hat{a}_1/a_1$).*

C Measurement Results

This appendix contains the measurement results for all of the tested subjects. Appendix C.1 will first show the efficiencies, leakage flow rates, power losses, and torque losses per unit at different operating speeds and pressure levels. Appendix C.2 will then show the same results, but grouped per pressure level p_2, so the different machines can be compared at each pressure. Section 4 explains in more detail what can be seen in each figure.

C.1 Results per Machine

The following pages contain the results for the measurements on all the tested subjects. The layout of these results is the same for all machines (also shown in Figure C.1):

- The top left corner contains a table with information about the machine, followed by some information about the point of operation where the maximum efficiency was measured.
- The top right corner shows a contour plot for the efficiencies at different operating pressures and speeds.
- The middle of the page contains two figures that present the leakage flow rate on the left, and the absolute power loss on the right.
- The bottom of the page contains two figures that present the torque loss at different operation conditions. The figure on the left shows this loss on a linear scale, the figure on the right shows the same loss but on a logarithmic scale.

In each of the torque loss and leakage figures, a line connects ascending speeds, measured at the same pressure p_2. A discontinued line means that a point is missing in the results. The colors of the lines are the same in each of the four figures, the legend of which can be found in the middle left figure.

Please note that there is a boundary around the efficiency contours. Points of operation outside of this boundary were either not measured, or could not be used for efficiency calculations. The latter can occur when the leakage is larger than the actual flow created by the displacement. In these cases an additional pump was used to compensate for these losses.

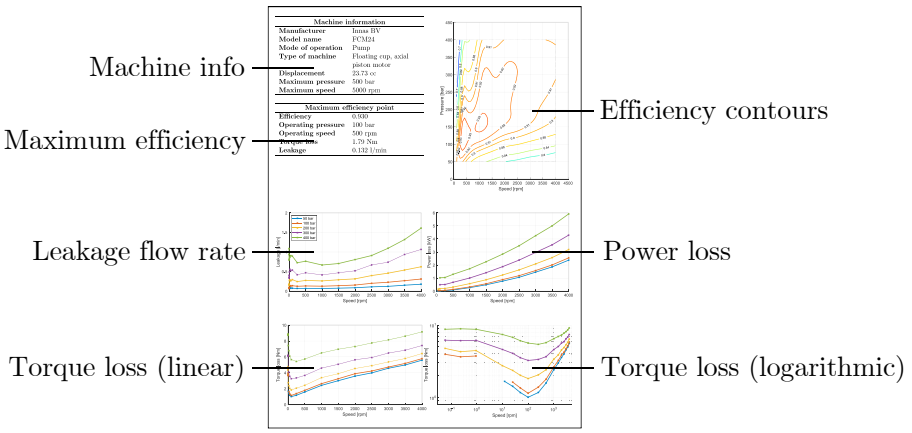

Figure C.1: *Layout of the measurement results shown on the following pages.*

Machine information	
Manufacturer	Rexroth
Model name	A4FM28
Mode of operation	Motor
Type of machine	Slipper type, axial piston motor
Displacement	27.75 cc
Return pressure	6.0 bar
Maximum pressure	400 bar
Maximum speed	4250 rpm

Maximum efficiency point	
Efficiency	0.912
Operating pressure	250 bar
Operating speed	1000 rpm
Torque loss	3.95 Nm
Leakage	0.194 l/min

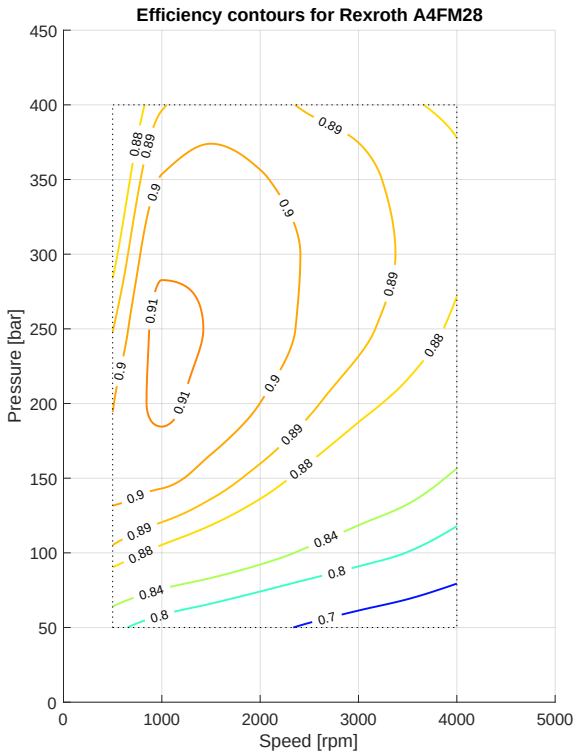

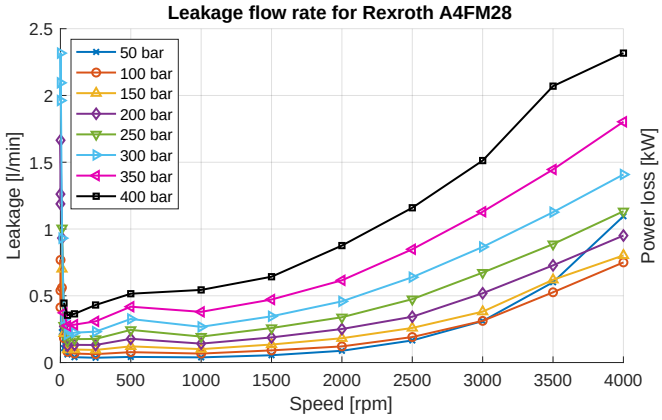

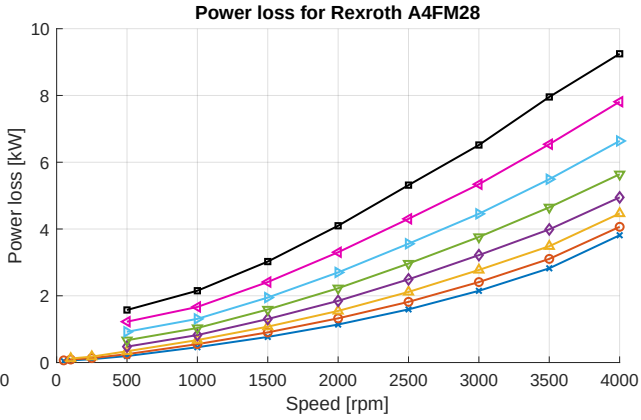

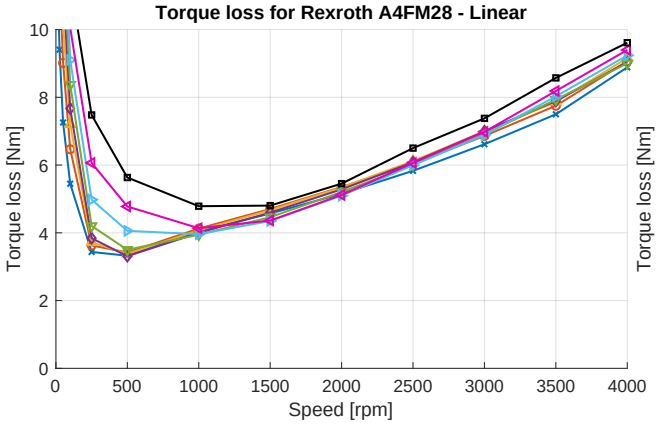

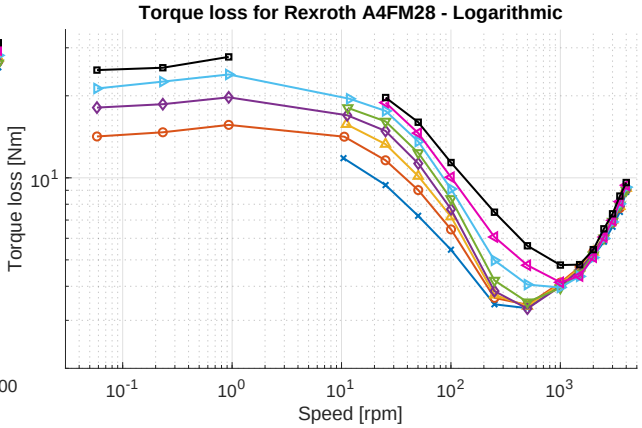

Machine information	
Manufacturer	KYB
Model name	MSF30
Mode of operation	Motor
Type of machine	Slipper type, axial piston motor
Displacement	30.17 cc
Return pressure	10.0 bar
Maximum pressure	250 bar
Maximum speed	2000 rpm

Maximum efficiency point	
Efficiency	0.922
Operating pressure	150 bar
Operating speed	1000 rpm
Torque loss	3.38 Nm
Leakage	0.602 l/min

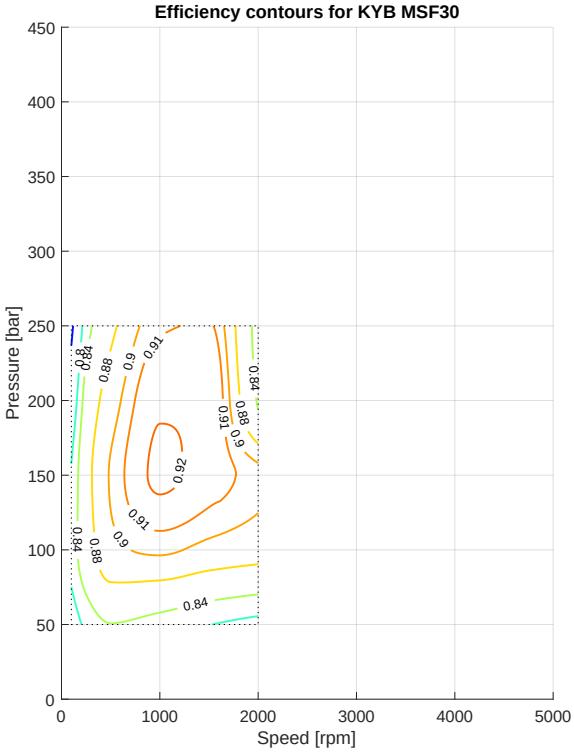

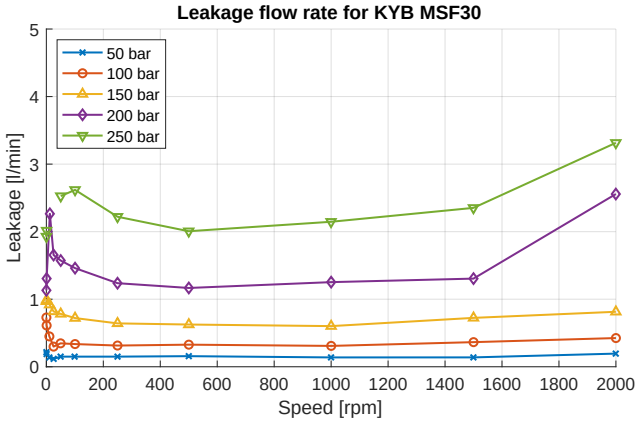

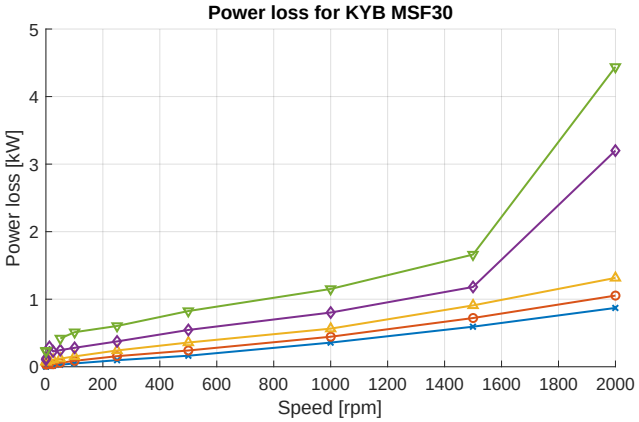

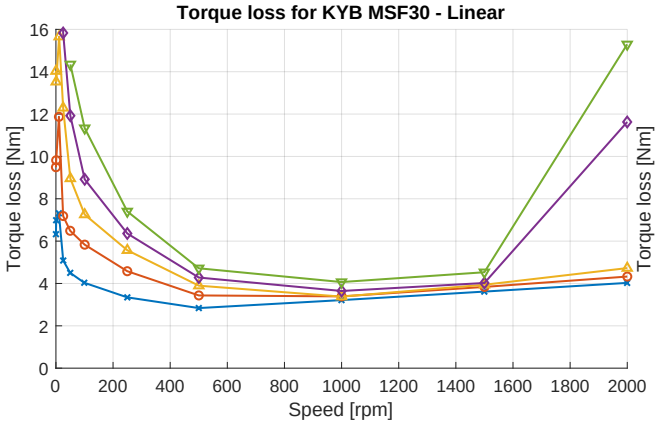

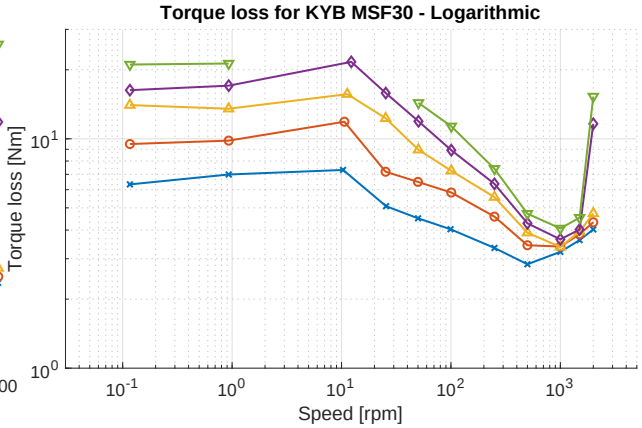

Machine information	
Manufacturer	Brevini
Model name	SH11CM030
Mode of operation	Motor
Type of machine	Bent-axis, axial piston motor
Displacement	31.89 cc
Return pressure	10.0 bar
Maximum pressure	430 bar
Maximum speed	4750 rpm

Maximum efficiency point	
Efficiency	0.947
Operating pressure	400 bar
Operating speed	2500 rpm
Torque loss	4.77 Nm
Leakage	1.062 l/min

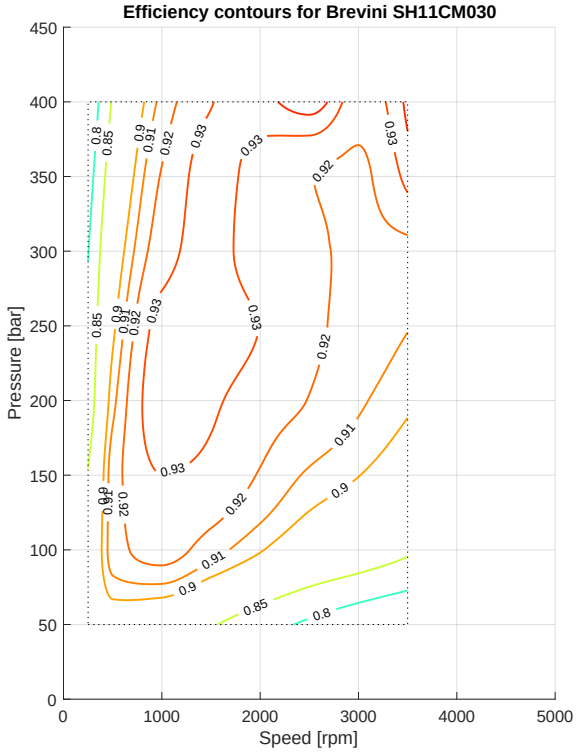

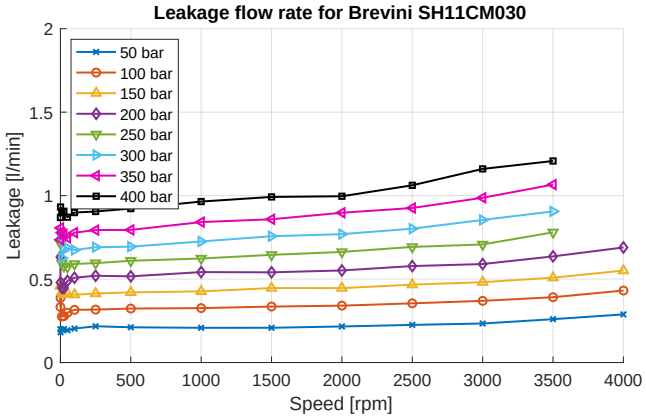

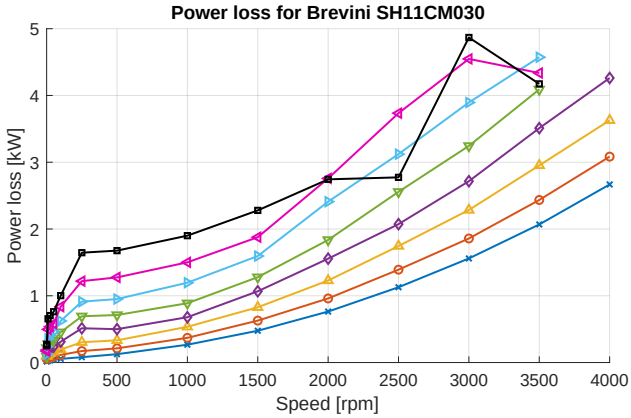

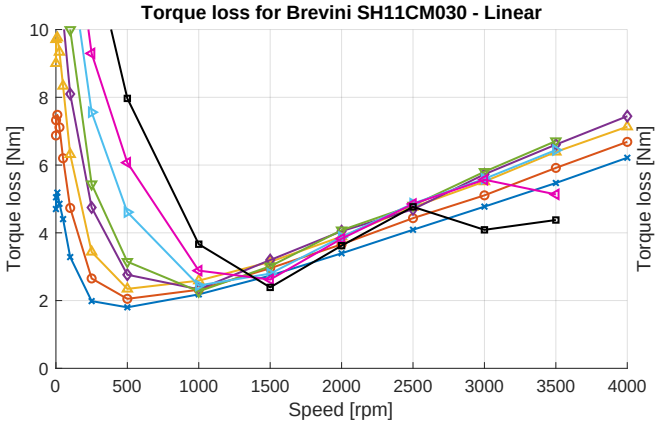

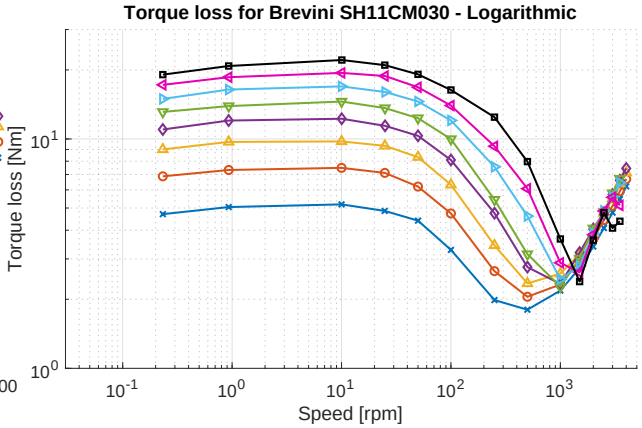

Machine information	
Manufacturer	Rexroth
Model name	A4FO28
Mode of operation	Pump
Type of machine	Slipper type, axial piston pump
Displacement	27.87 cc
Supply pressure	6.0 bar
Maximum pressure	400 bar
Maximum speed	3750 rpm

Maximum efficiency point	
Efficiency	0.916
Operating pressure	200 bar
Operating speed	1500 rpm
Torque loss	6.57 Nm
Leakage	0.612 l/min

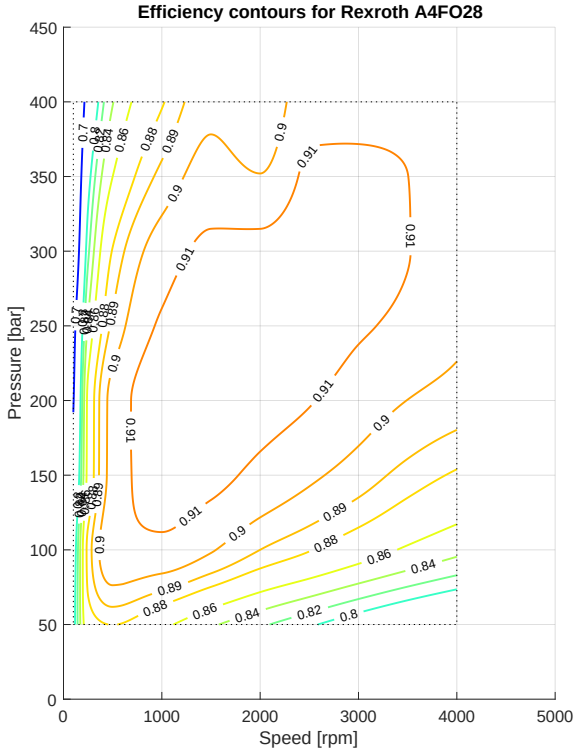

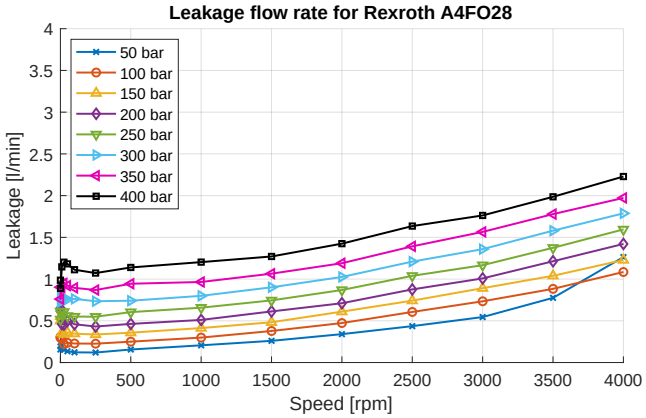

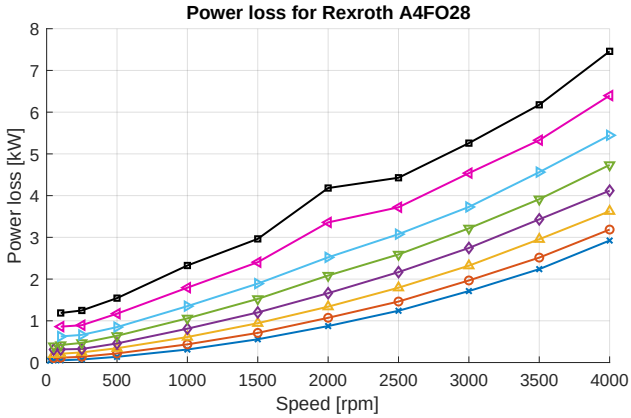

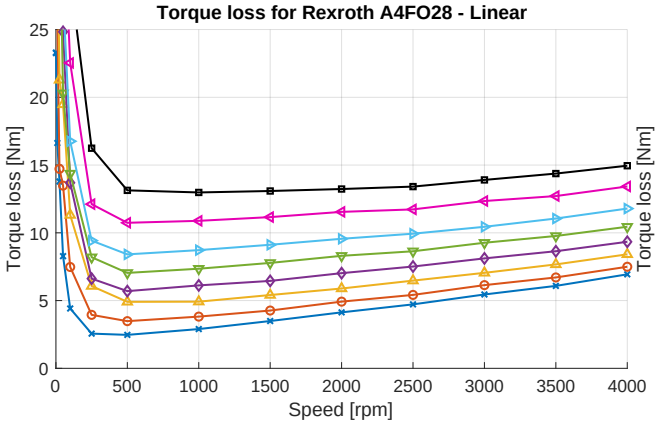

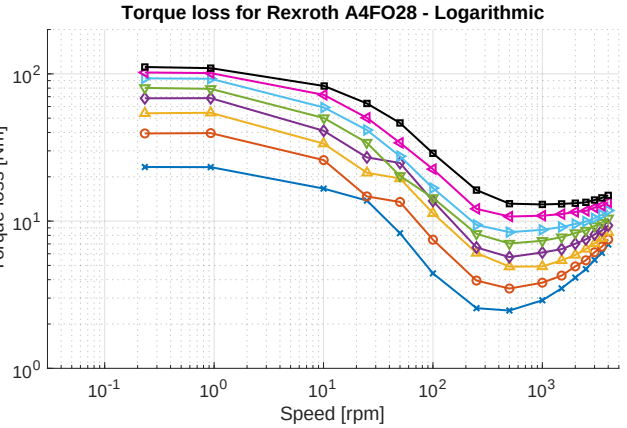

Machine information	
Manufacturer	Moog
Model name	RKP32
Mode of operation	Pump
Type of machine	Slipper type, radial piston pump
Displacement	32.66 cc
Supply pressure	1.4 bar
Maximum pressure	350 bar
Maximum speed	2750 rpm

Maximum efficiency point	
Efficiency	0.875
Operating pressure	50 bar
Operating speed	500 rpm
Torque loss	1.35 Nm
Leakage	1.049 l/min

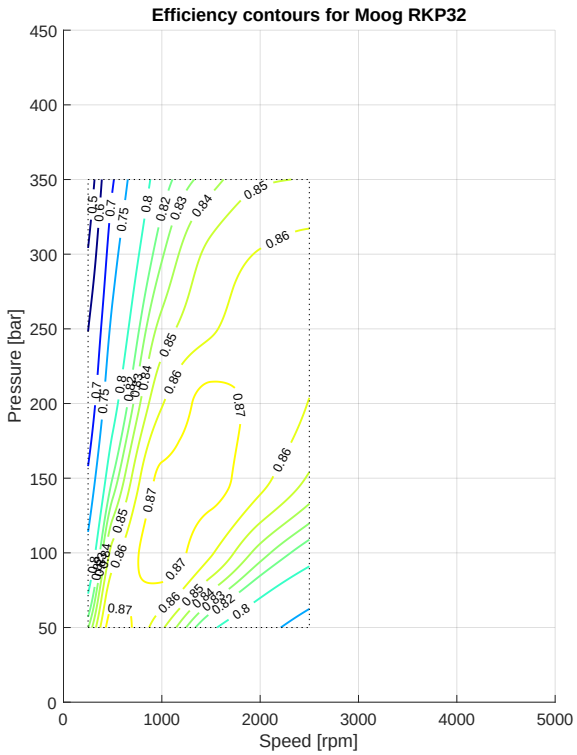

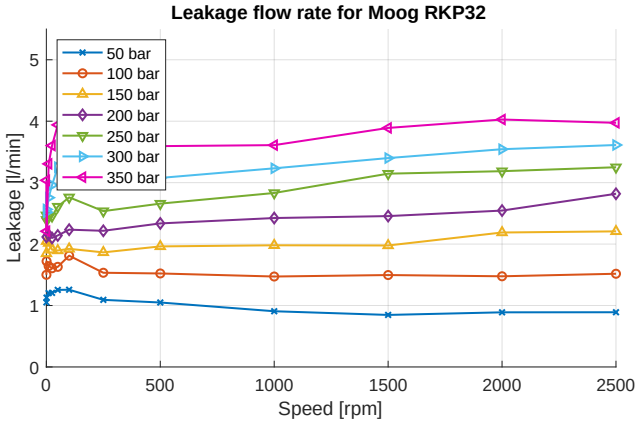

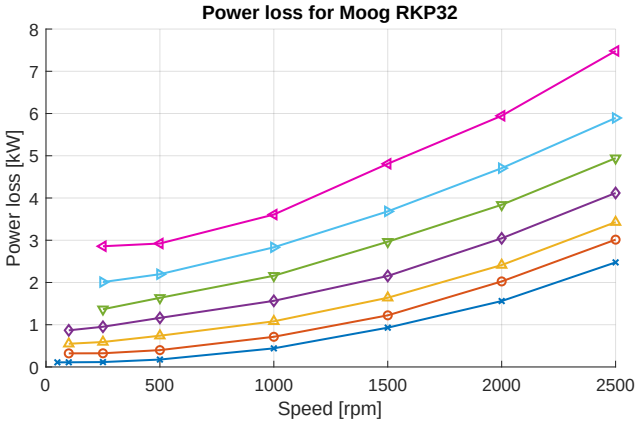

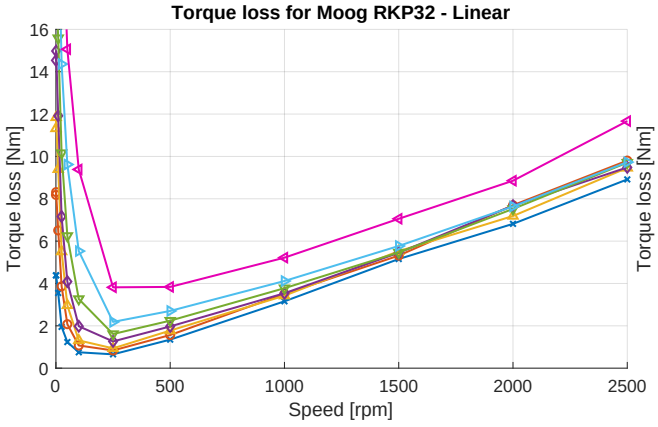

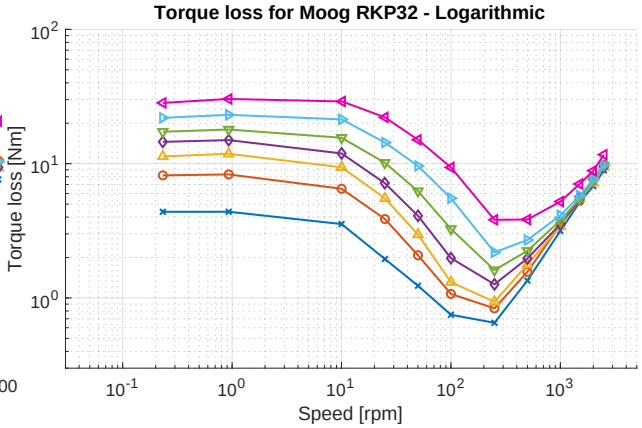

Machine information	
Manufacturer	Eckerle
Model name	EIPH3-025
Mode of operation	Pump
Type of machine	Internal gear pump
Displacement	24.31 cc
Supply pressure	1.4 bar
Maximum pressure	330 bar
Maximum speed	3200 rpm

Maximum efficiency point	
Efficiency	0.919
Operating pressure	250 bar
Operating speed	1500 rpm
Torque loss	5.74 Nm

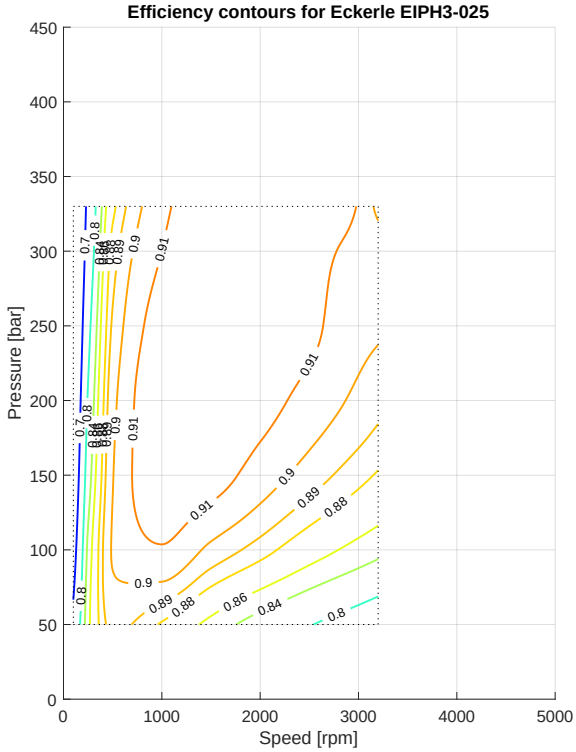

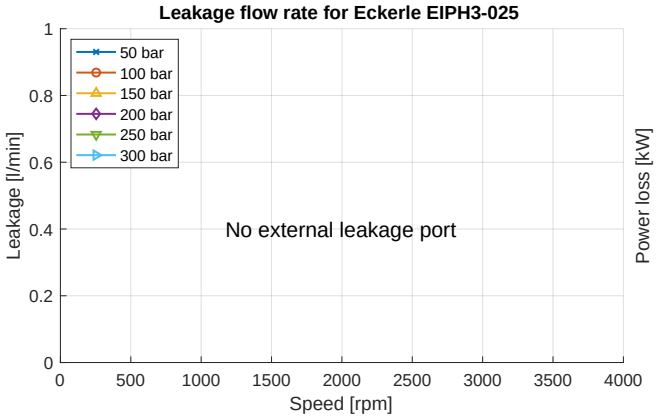

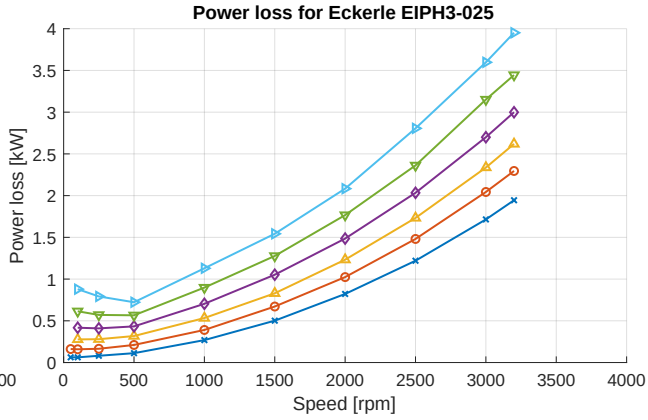

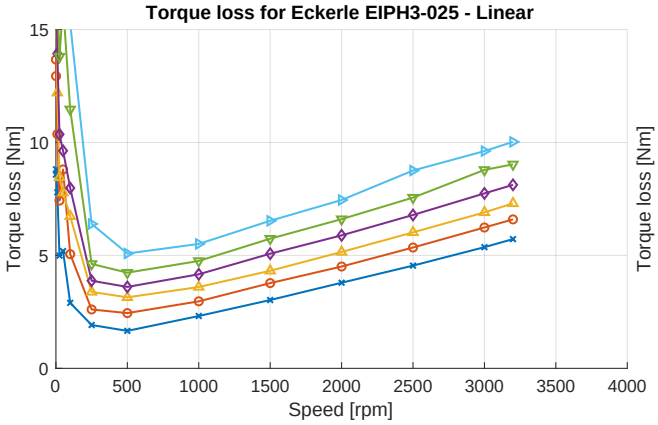

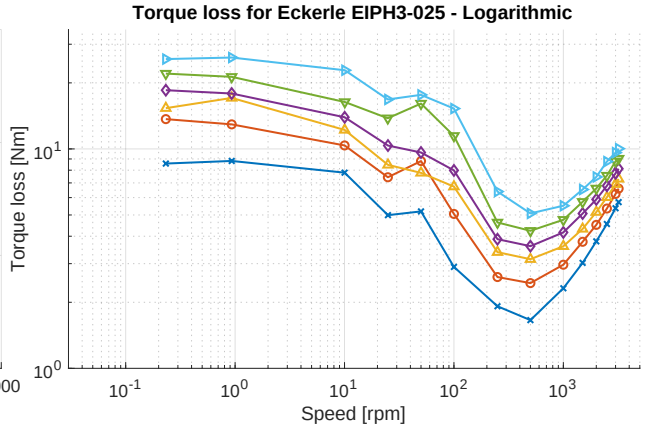

Machine information	
Manufacturer	Marzocchi
Model name	ELI2-D-25.7
Mode of operation	Pump
Type of machine	External gear pump
Displacement	25.41 cc
Supply pressure	1.8 bar
Maximum pressure	210 bar
Maximum speed	3000 rpm

Maximum efficiency point	
Efficiency	0.915
Operating pressure	200 bar
Operating speed	1500 rpm
Torque loss	6.28 Nm

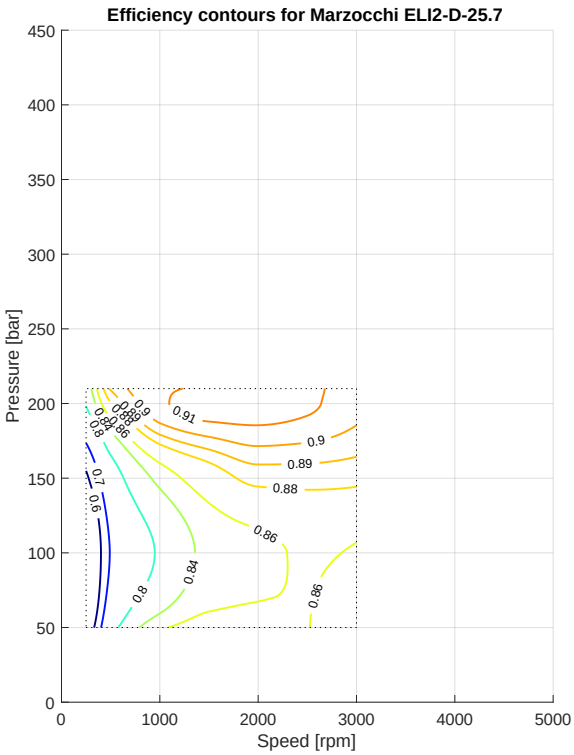

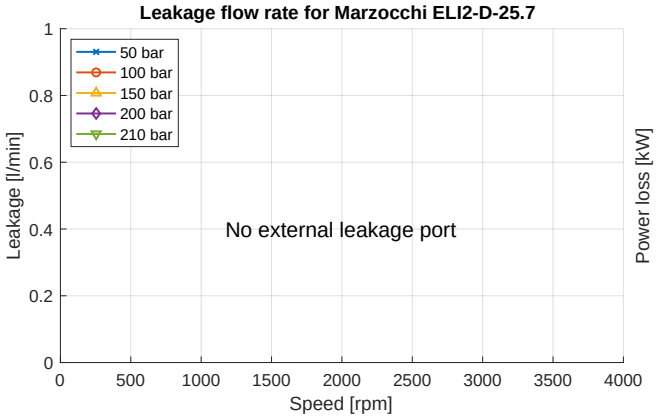

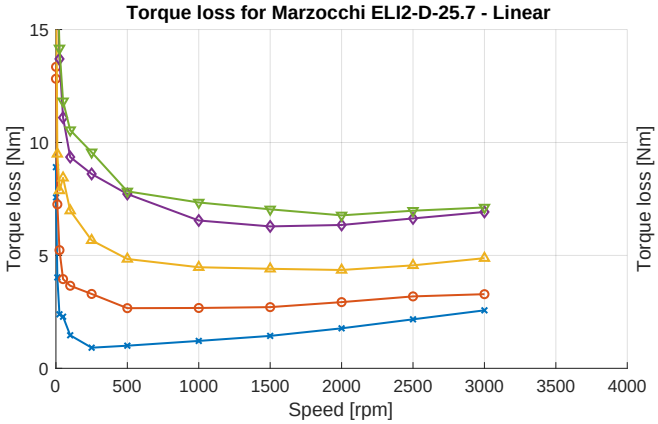

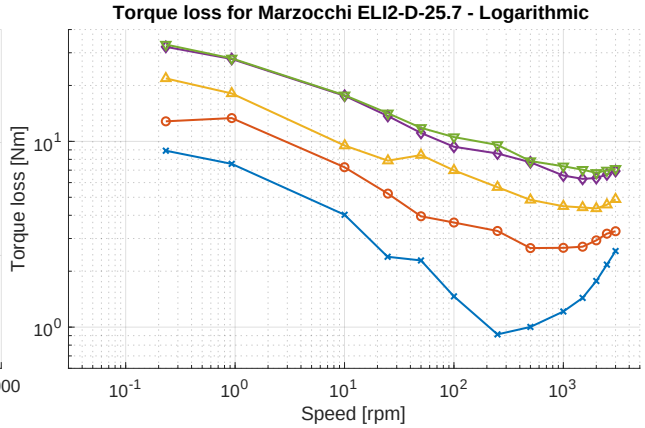

Machine information	
Manufacturer	Innas BV
Model name	FC24
Mode of operation	Pump
Type of machine	Floating cup, axial piston pump
Displacement	23.65 cc
Supply pressure	6.0 bar
Maximum pressure	500 bar
Maximum speed	5000 rpm

Maximum efficiency point	
Efficiency	0.996
Operating pressure	50 bar
Operating speed	100 rpm
Torque loss	0.20 Nm
Leakage	0.023 l/min

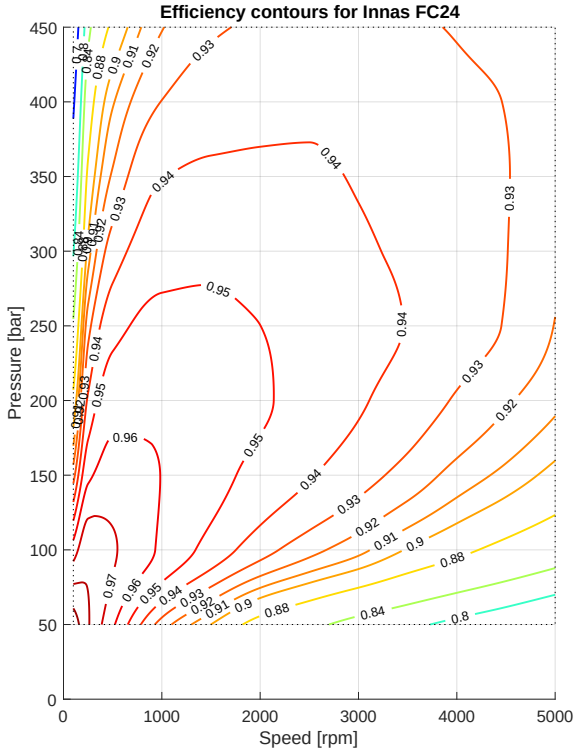

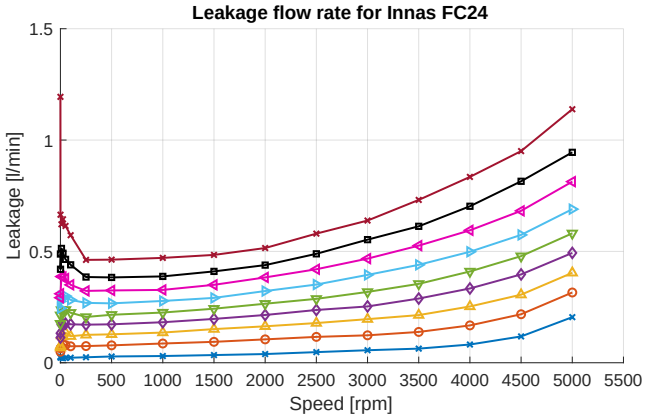

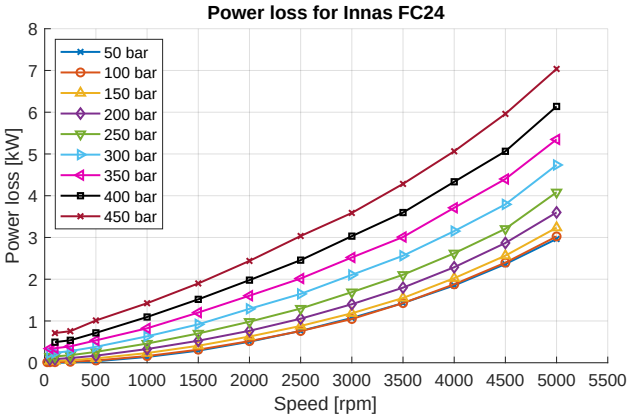

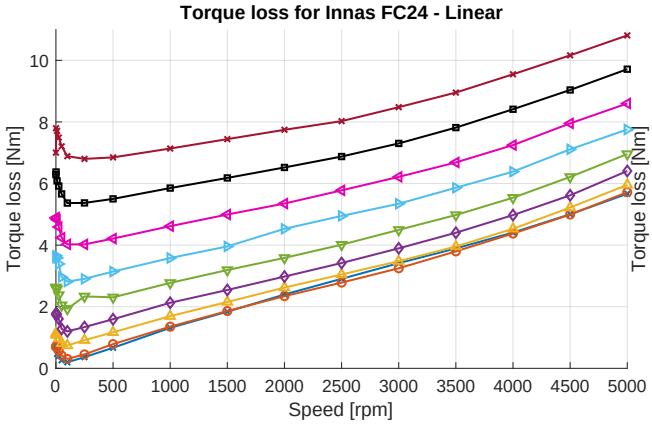

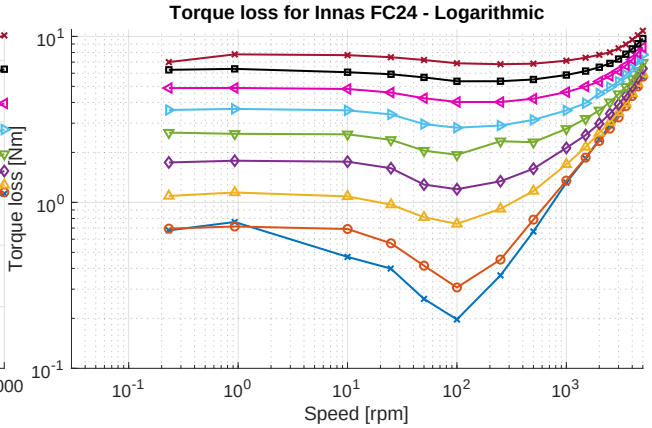

C.2 Results per Pressure Level

This appendix contains the following results at pressure p_2 equals 50 to 400 bar, with 50 bar increments:

- Overall efficiency (η_t) in Figure C.2
- Normalized torque loss ($\hat{T}_{loss}$) in figures C.3 and C.4
- Leakage flow rate (Q_3) in Figure C.5

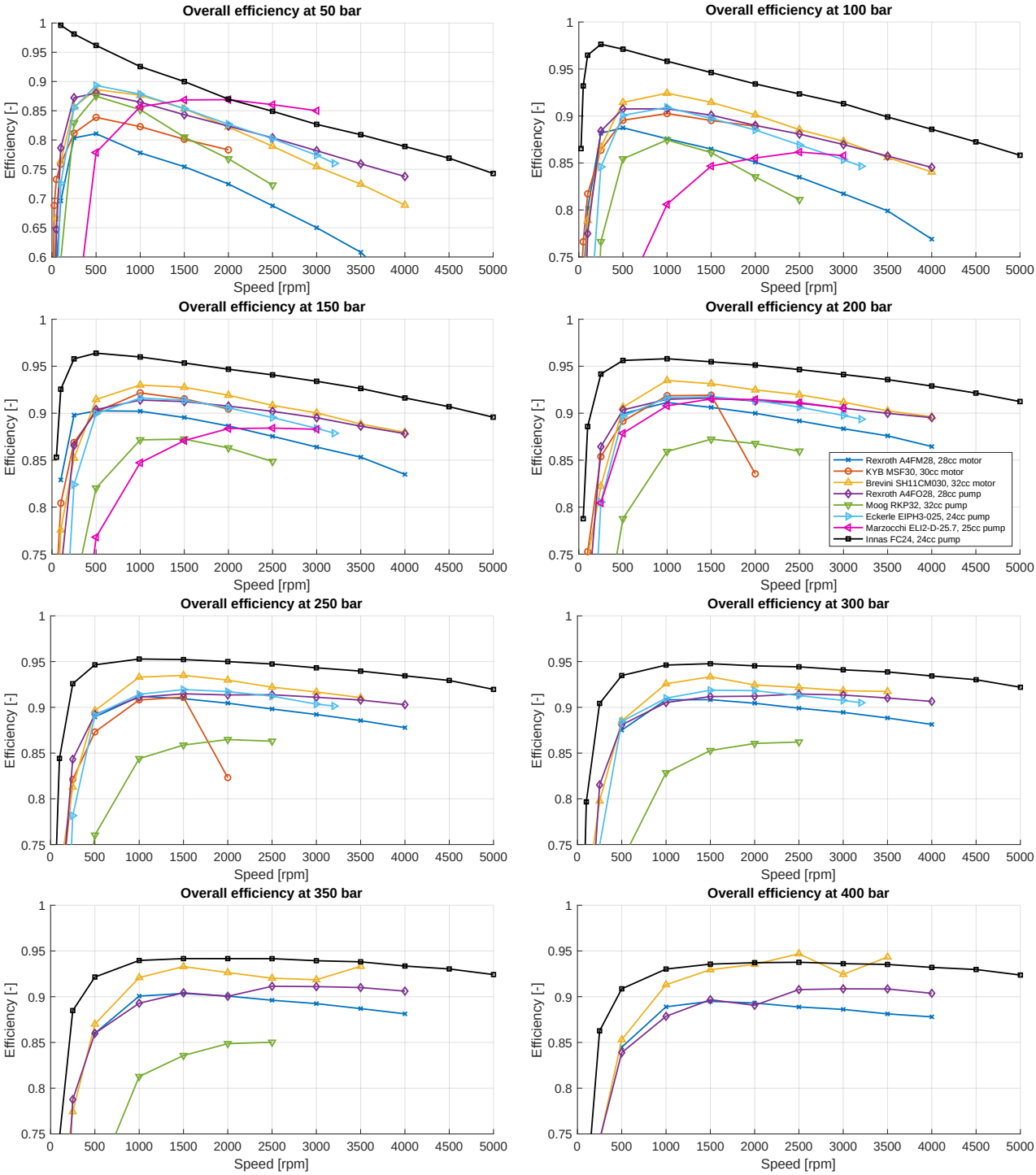

Figure C.2: *Comparison between the overall efficiency for all of the machines with pressure p_2 ranging from 50 to 400 bar.*

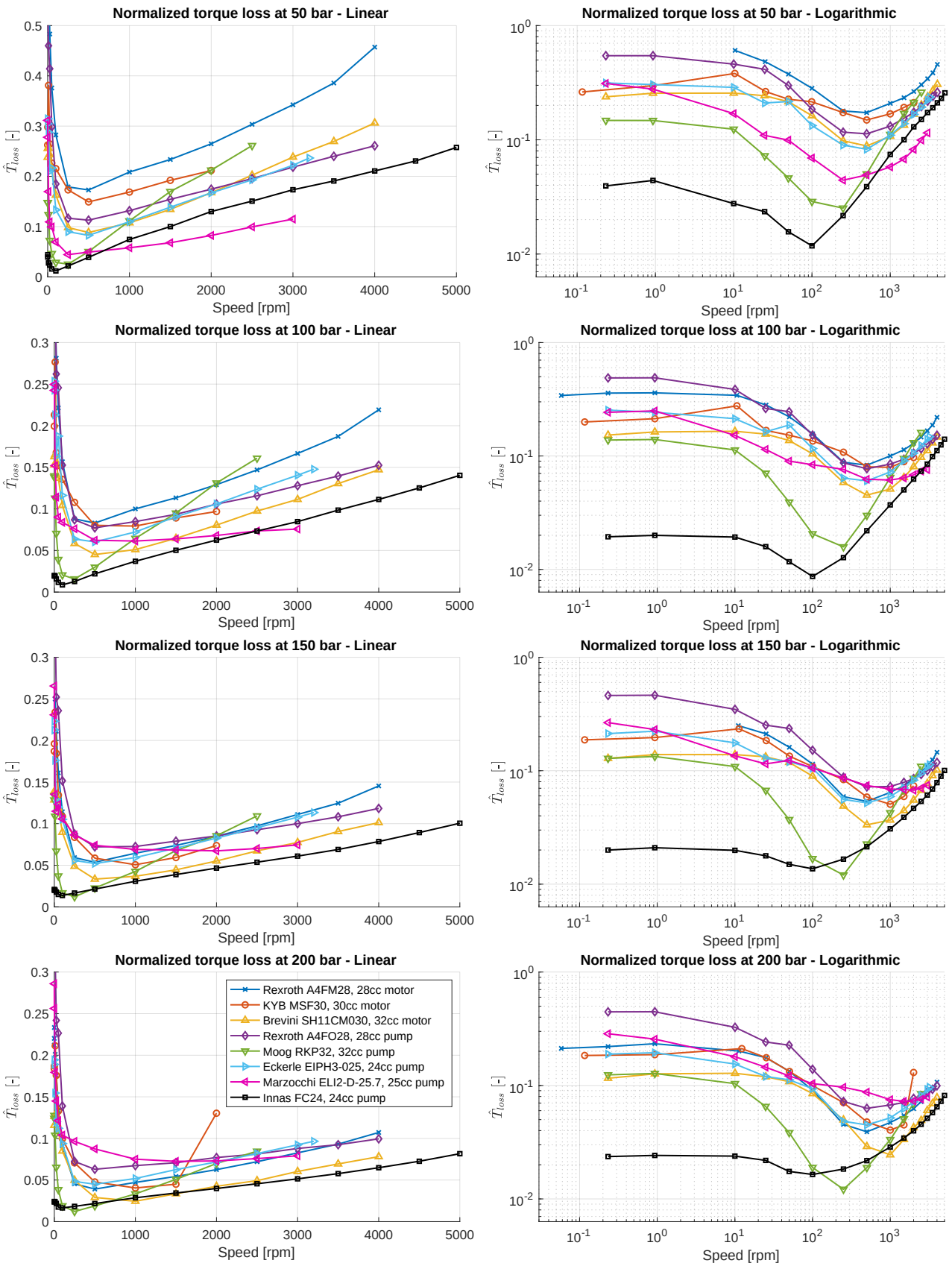

Figure C.3: *Comparison between the normalized torque losses for all of the machines with pressure p_2 ranging from 50 to 200 bar.*

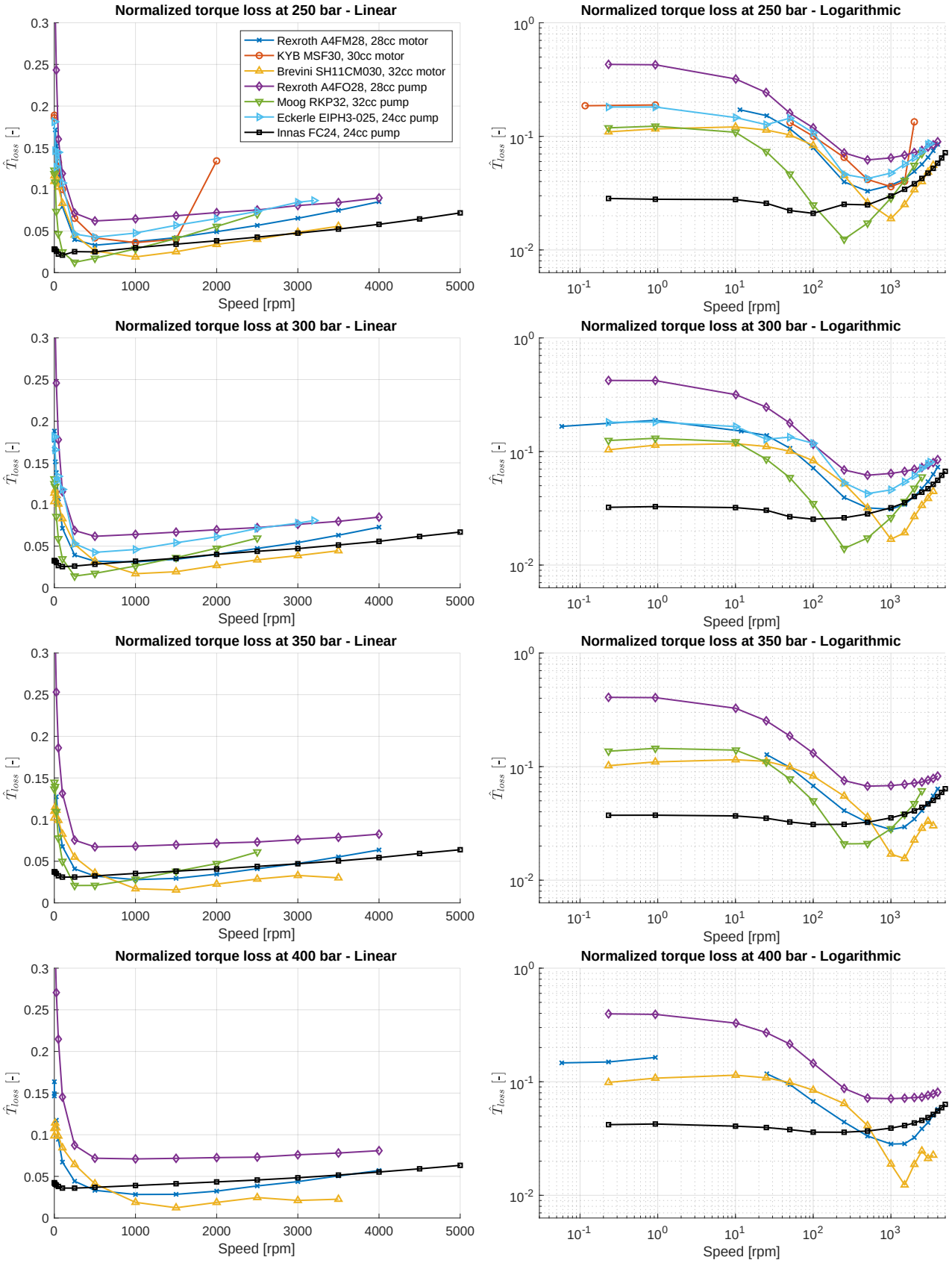

Figure C.4: *Comparison between the normalized torque losses for all of the machines with pressure p_2 ranging from 250 to 400 bar.*

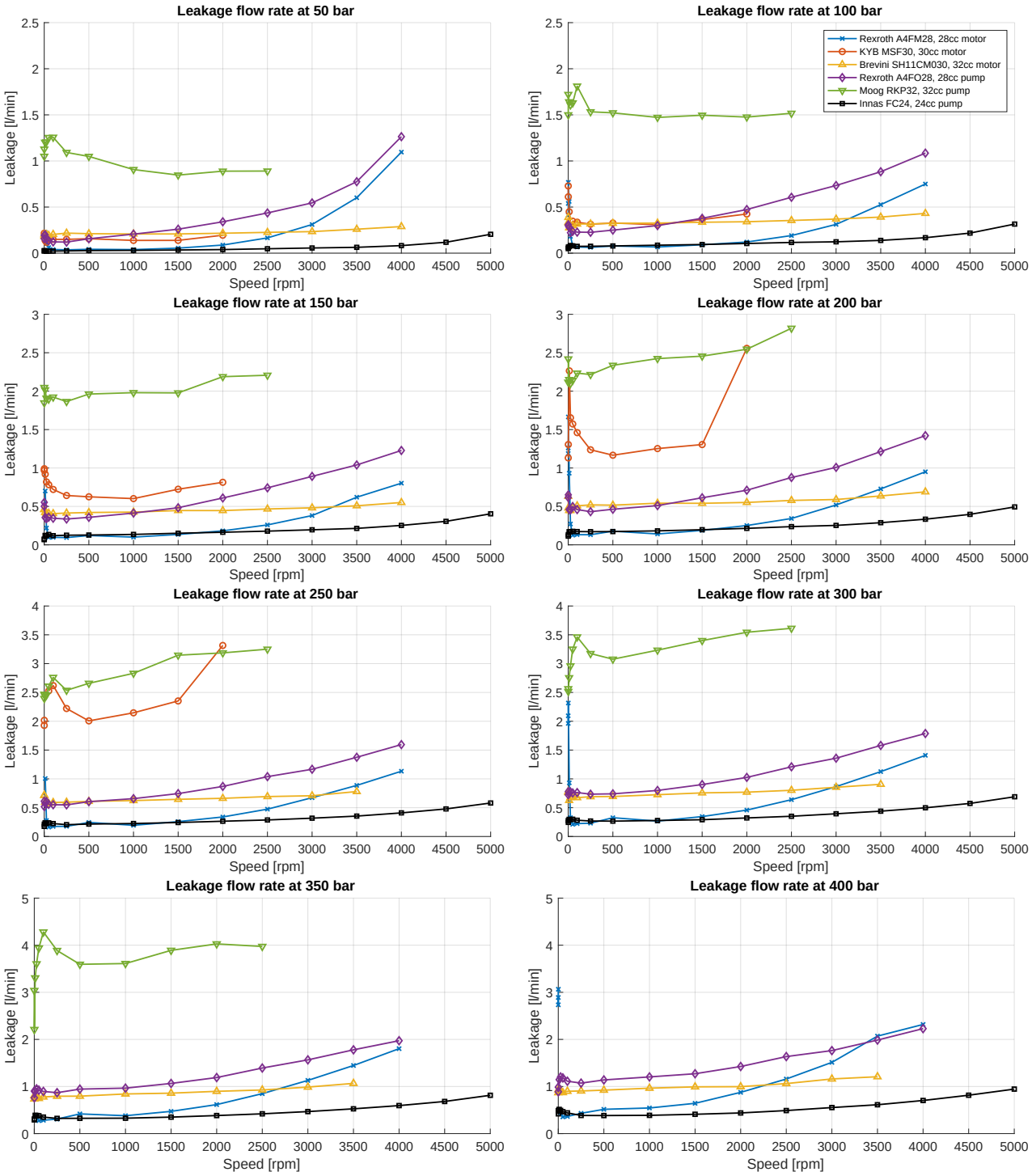

Figure C.5: *Comparison between the leakage flow rate for all of the machines with pressure p_2 ranging from 50 to 400 bar.*

D Low Speed Measurements Comparisons

As mentioned in Section 2.2, the very low speed measurements allow for a precise comparison between different test runs. Figures D.1 to D.3 present three comparisons between the torque loss of a test subject while changing one of the conditions.

Figure D.1 shows the measured torque loss for the Innas machine driven as a pump at 300 bar. This pump has 24 pistons, which is clearly visible by the 24 roughly equal segments that make up one full rotation. The difference between the different lines is that the pump was rotating at three different speeds. Scaling the results for the three measurements to the shaft angle, we see a very close resemblance between the tests at 0.931, 0.233, and 0.058 rpm.

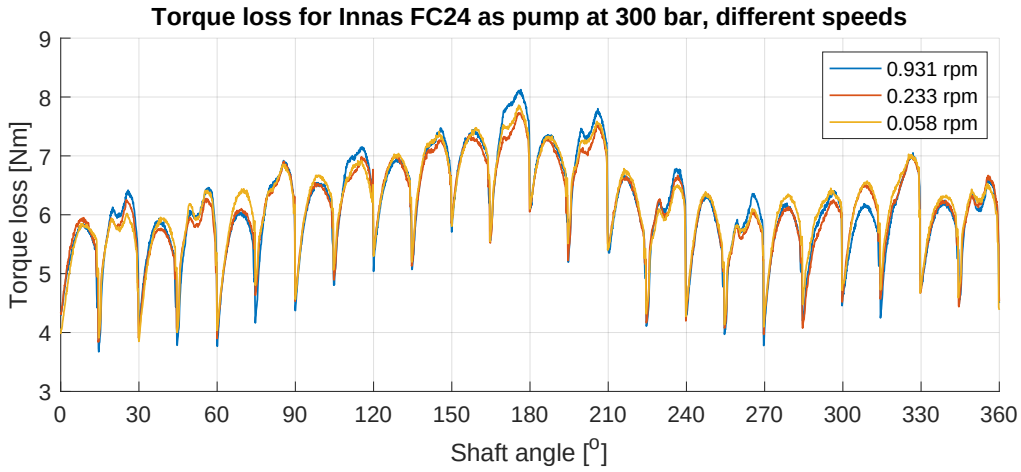

Figure D.1: *Torque loss per rotational position for the Innas FC24 driven as a pump at different speeds.*

Figure D.2 shows the measured normalized torque loss for the Brevini machine driven as a motor at 0.233 rpm. This motor has seven pistons, which can again be seen by the seven roughly equal segments that make up one full rotation. The difference between the shown results is that the pump was driven at different pressure levels p_2. The figure shows that although the amount of normalized torque loss decreases with increasing pressure, the shape of the torque loss is very similar at the angular positions of the shaft. This shape is a unique and inherent property for each machine, as the smallest differences in the production of a pump or motor can account for a very distinctive shape in the torque loss.

Figure D.3 shows the measured torque loss for the Rexroth motor during a cold start. The figure shows the results of tests performed after various standstill times of the test object. In each of the tests, the motor is operated at a speed of 0.233 rpm and a pressure of 300 bar. The first test was performed immediately following a warmup procedure. The other tests were made after one hour, one day, and three days of standstill respectively, during which the oil and the motor cooled down to roughly 25°C and 20°C. Having the motor standing still for some time decreases the amount of oil still being present in the gap between the portplate and barrel, which greatly influences the friction conditions of the sliding bearing interfaces at near zero operating speeds. In Figure D.3 we see a significant increase in the breakaway torque loss after waiting one hour by roughly 25%. After this first hour however, the difference becomes far less noticeable as seen by the three lines following roughly the same torque loss during these first 200 seconds.

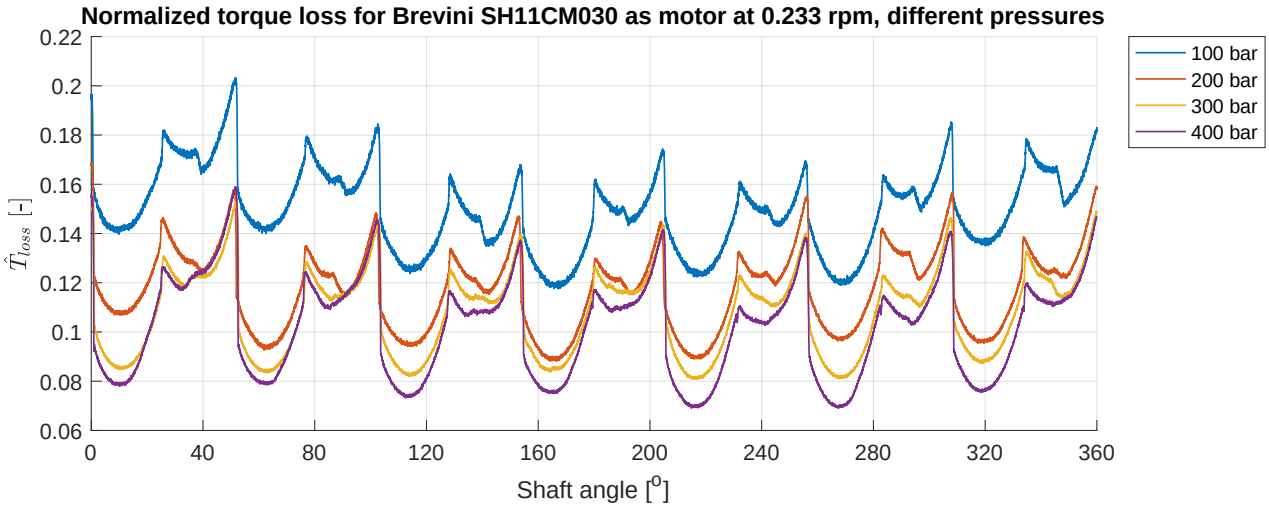

Figure D.2: *Normalized torque loss per rotational position for the Brevini SH11CM030 driven as a motor at different pressures.*

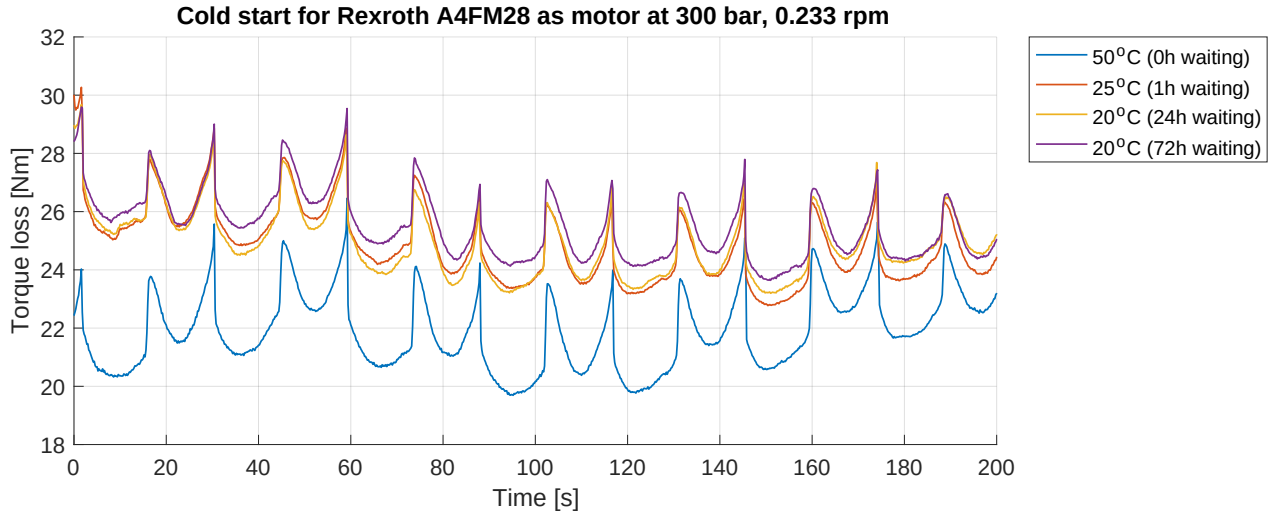

Figure D.3: *Effect of standstill on the torque loss for the Rexroth A4FM28 driven as a motor at 0.233 rpm.*